

Cobalt Electrolyte/Dye Interactions in Dye-Sensitized Solar Cells: A Combined Computational and Experimental Study

Edoardo Mosconi,[†] Jun-Ho Yum,[‡] Florian Kessler,[‡] Carlos J. Gómez García,[§] Cristiano Zuccaccia,[⊥] Antonio Cinti,^{†,⊥} Mohammad K. Nazeeruddin,[‡] Michael Grätzel,[‡] and Filippo De Angelis^{*,†}

[†]Computational Laboratory for Hybrid and Organic Photovoltaics, Istituto CNR di Scienze e Tecnologie Molecolari, via Elce di Sotto 8, 06123 Perugia, Italy

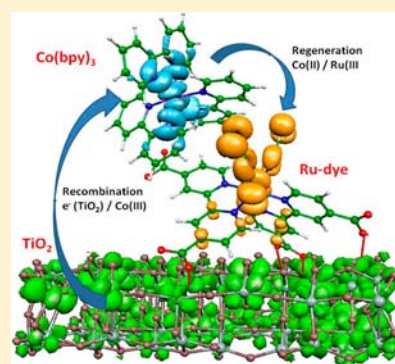
[‡]Laboratory for Photonics and Interfaces, Institution of Chemical Sciences and Engineering, School of Basic Sciences, Swiss Federal Institute of Technology, CH-1015 Lausanne, Switzerland

[§]Instituto de Ciencia Molecular Parque Científico, Universidad de Valencia, C/José Beltrán, 2 46980 Paterna (Valencia), Spain

[⊥]Dipartimento di Chimica, Università degli Studi di Perugia, via Elce di Sotto 8, 06123 Perugia, Italy

Supporting Information

ABSTRACT: We report a combined experimental and computational investigation to understand the nature of the interactions between cobalt redox mediators and TiO₂ surfaces sensitized by ruthenium and organic dyes, and their impact on the performance of the corresponding dye-sensitized solar cells (DSSCs). We focus on different ruthenium dyes and fully organic dyes, to understand the dramatic loss of efficiency observed for the prototype Ru(II) N719 dye in conjunction with cobalt electrolytes. Both N719- and Z907-based DSSCs showed an increased lifetime in iodine-based electrolyte compared to the cobalt-based redox shuttle, while the organic D21L6 and D25L6 dyes, endowed with long alkoxy chains, show no significant change in the electron lifetime regardless of employed electrolyte and deliver a high photovoltaic efficiency of 6.5% with a cobalt electrolyte. Ab initio molecular dynamics simulations show the formation of a complex between the cobalt electrolyte and the surface-adsorbed ruthenium dye, which brings the [Co(bpy)₃]³⁺ species into contact with the TiO₂ surface. This translates into a high probability of intercepting TiO₂-injected electrons by the oxidized [Co(bpy)₃]³⁺ species, lying close to the N719-sensitized TiO₂ surface. Investigation of the dye regeneration mechanism by the cobalt electrolyte in the Marcus theory framework led to substantially different reorganization energies for the high-spin (HS) and low-spin (LS) reaction pathways. Our calculated reorganization energies for the LS pathways are in excellent agreement with recent data for a series of cobalt complexes, lending support to the proposed regeneration pathway. Finally, we systematically investigate a series of Co(II)/Co(III) complexes to gauge the impact of ligand substitution and of metal coordination (tris-bidentate vs bis-tridentate) on the HS/LS energy difference and reorganization energies. Our results allow us to trace structure/property relations required for further development of cobalt electrolytes for DSSCs.



1. INTRODUCTION

Dye-sensitized solar cells (DSSCs) are promising hybrid/organic photovoltaic devices for high-efficiency, low-cost solar energy conversion.^{1–5} In typical DSSCs, a mesoporous film of TiO₂ nanoparticles is sensitized with light-harvesting dyes, either organic or metallorganic, which in most applications are surrounded by a redox mediator^{6–8} in an organic solvent, typically acetonitrile.^{9,10} The classic redox mediator in DSSCs is the I₃[−]/I[−] redox couple, which in conjunction with Ru(II) dyes delivers certified efficiencies of 11.4%.¹¹ Fully organic dyes are also nicely performing with I₃[−]/I[−] electrolytes, with efficiencies exceeding 10%.¹² The I₃[−]/I[−] redox couple, however, is also known to have limitations due to its complex redox chemistry and to its corrosive nature, which complicates large-scale DSSCs production.^{11–16}

In recent reports, organic redox mediators, such as disulfide/thiolate,¹⁷ McMT/BM,¹⁸ and TMFDS²⁺/TMTU,^{19,20} have

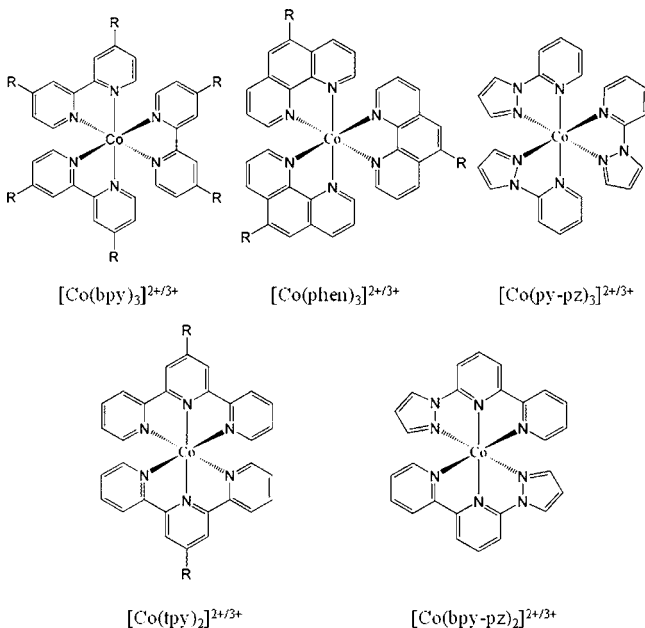
been investigated as alternatives to the conventional I₃[−]/I[−] redox couple. These systems, however, are similar to I₃[−]/I[−] in complexity because they involve the transfer of two electrons in their overall redox reactions. In contrast, mono-electronic metallorganic redox couples such as ferrocene/ferrocenium,²¹ Ni(III)/Ni(IV),²² and Co(II)/Co(III) complexes^{23–39} usually show simpler kinetics and may require a smaller energy expenditure for the dye regeneration process, reducing the associated loss of open-circuit voltage. Among these alternative redox mediators, tris-chelated cobalt(II)/(III) complexes, such as [Co(bpy)₃]^{2+/3+}, [Co(phen)₃]^{2+/3+}, or [Co(py-pz)₃]^{2+/3+} (bpy = bipyridine, phen = phenanthroline, py-pz = pyridine-pyrazole), or bis-chelated complexes, such as [Co(bpy-pz)₂]^{2+/3+} or [Co(tpy)₂]^{2+/3+} (bpy-pz = bipyridine-pyrazole,

Received: August 8, 2012

Published: October 31, 2012

tpy = terpyridine) (Scheme 1), have provided the highest DSSC performances. A Zn(II)–porphyrin/organic dye cocktail

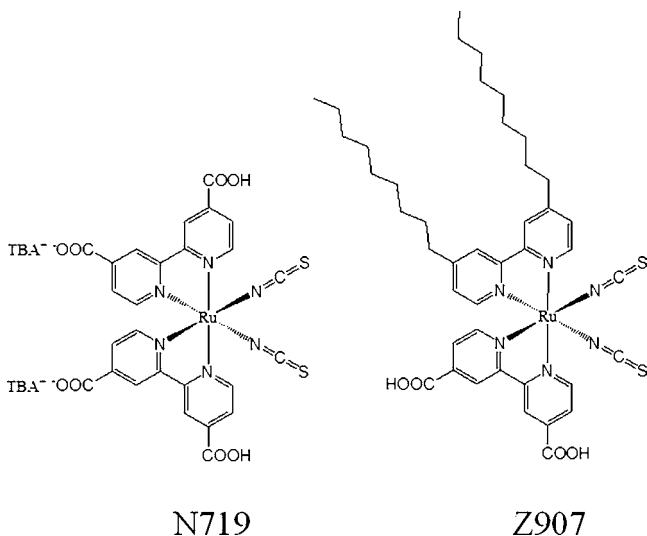
Scheme 1. Chemical Structures of the Cobalt Complexes Investigated in This Work



in conjunction with $[\text{Co}(\text{bpy})_3]^{2+/3+}$ provided the new DSSCs record efficiency of $\sim 12.3\%$ under AM1.5 conditions.²⁸

Several promising results^{25,27,32,34} have been obtained using Co(II)/Co(III) redox mediators with organic dyes. In particular, it was reported that the sterically congested D35 and Y123 organic dyes,^{25,27,32} used in conjunction with a $[\text{Co}(\text{bpy-pz})_2]^{2+/3}$ electrolyte, led to photovoltaic efficiency of $\sim 10\%$, with DSSCs open-circuit voltage exceeding 1 V.²⁷ Quite surprisingly, the prototypical high-efficiency Ru(II) N719 dye (Scheme 2) delivered dramatically low photovoltaic efficiency, $\sim 2\%$, when using a Co(II)/Co(III) redox mediator,^{24,29} while the same system provided high efficiency, exceeding 11%, when

Scheme 2. Chemical Structures of the Ruthenium N719 and Z907 Dyes

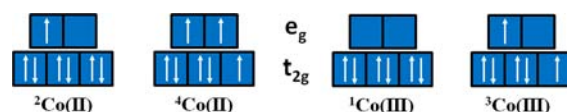


coupled to the I_3^-/I^- redox couple.³⁷ Interestingly, not all Ru(II) dyes performed poorly with Co(II)/Co(III) redox mediators; the Ru(II) Z907 dye (Scheme 2), endowed with long nonyl chains, delivered similar efficiency with Co(II)/Co(III) ($\eta = 6.5\%$) and I_3^-/I^- redox couples ($\eta = 7.7\%$).²⁹ Surprisingly, earlier kinetics measurements demonstrated that dye regeneration by cobalt electrolytes was faster with the less efficient N719 dye than with the most performing Z907 dye.²⁴

The reason for this widely varying efficiency of DSSCs employing Ru(II) dyes and Co(II)/Co(III) electrolytes is still a matter of debate.^{24,29,30} Considering the different N719 and Z907 dye structures, the former carrying four carboxylic/carboxylate groups only partly screened by TBA counterions,³⁸ and the higher regeneration rates of N719, Grätzel and co-workers ascribed the low N719 efficiency to the possible formation of ion-pairs between the negatively charged, TiO_2 -adsorbed N719 dye^{39,40} and the oxidized Co(III) electrolyte species.^{24,30} Ion-pair formation may increase the probability of intercepting TiO_2 electrons by Co(III) species, consequently decreasing the charge collection efficiency and limiting the DSSCs photocurrent and photovoltage. Recently, the good efficiency of Z907 with Co(II)/Co(III) electrolytes was associated to a surface-blocking effect, whereby the long alkyl dye chains would form a compact dye layer, possibly impeding the close approach of the Co(III) species to the semiconductor surface.²⁹ A similar effect explained the high performance of organic dyes with bulky substituents on the donor moiety.^{25,27,32} In both cases, shifting the distribution of Co(III) ions away from the semiconductor surface seems to be key for high efficiency.

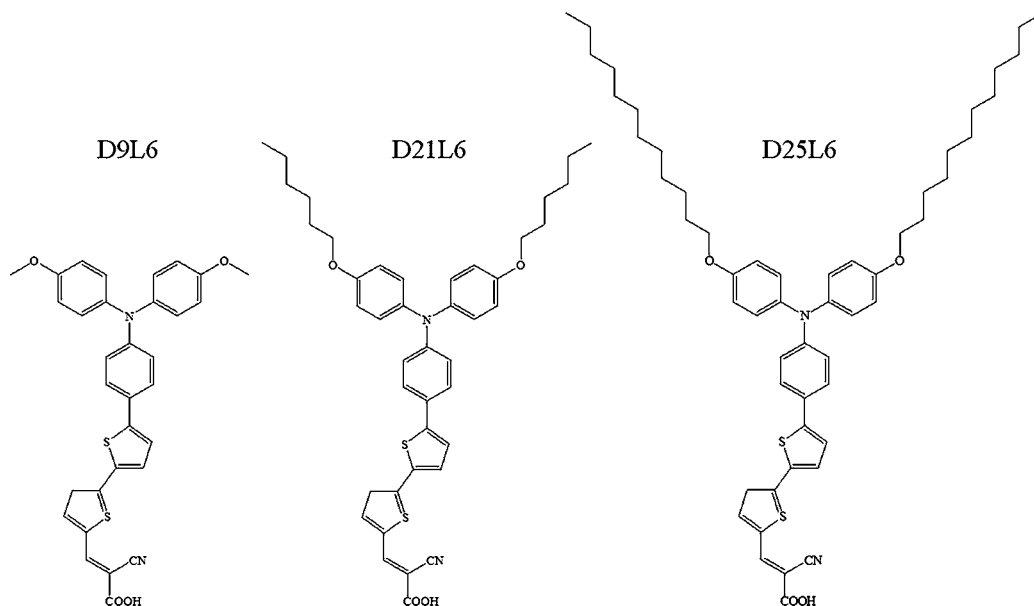
Another interesting and largely unexplored aspect in DSSCs based on cobalt electrolytes concerns the oxidized dye regeneration mechanism by Co(II) ions. Co(II) complexes, having a d^7 electronic configuration, are characterized by two low-lying electronic states of different spin-multiplicities, i.e., the doublet and the quartet states. The low-spin (LS) doublet state, $^2\text{Co}(\text{II})$, has a $(t_{2g})^6/(e_g)^1$ electron configuration, while the quartet high-spin (HS) state, $^4\text{Co}(\text{II})$, has a $(t_{2g})^5/(e_g)^2$ electronic configuration⁴¹ (see Scheme 3). Co(III) complexes, with d^6 electron configuration, are generally LS, with the triplet state lying at higher energy.

Scheme 3. Electronic Configuration of Co(II) Ions in Doublet and Quartet Spin States and of Co(III) Ions in Singlet and Triplet Spin States



As reported in the literature,^{41,42} at room temperature the $[\text{Co}(\text{bpy})_3]^{2+}$ complex is mainly present in its HS state. For the related $[\text{Co}(\text{tpy})_2]^{2+}$ complex, a LS state was found to be favored,⁴¹ this state being stabilized by Jahn–Teller distortion of the axial ligands.⁴¹ Since dye regeneration consists of electron transfer from the $^2,4\text{Co}(\text{II})$ complexes to the oxidized dye, giving the Co(III) complex, both HS and LS Co(II) could, in principle, contribute to the dye regeneration reaction pathway. Moreover, evaluation of the reorganization energy (λ) of the HS and LS species can be useful to estimate the kinetics of the regeneration process,⁴³ described in the Marcus theory framework.⁴⁴

Scheme 4. Chemical Structures of the Organic D9L6, D21L6, and D25L6 Dyes



Electron-transfer processes concerning the oxidation of $^{2,4}\text{Co(II)}$ to Co(III) complexes in solution have been experimentally and computationally investigated in several works.^{45–57} In particular, the self-exchange reaction of $[\text{Co}(\text{NH}_3)_6]^{2+/3+}$ complexes was deeply investigated.^{46–49} Moreover, kinetics measurements have been carried out to study the photoinduced electron-transfer processes involving covalently linked and not linked Ru(II) and Co(III) polypyridyl complexes in solution.^{50–57} The overall picture extracted from these works points out that both spin restrictions and nuclear reorganization factors significantly contribute to the retardation of the rate of the electron-transfer process.⁵⁷ The $\text{Ru(III)} \rightarrow \text{Ru(II)}$ recovery of covalently linked ruthenium/cobalt polypyridyl complexes was found to be much faster for Co(II) ions in the LS state than in the HS state,^{50,51} with the smaller intramolecular reorganization for the LS pathway being responsible for the faster electron transfer.^{50,51,57} It was also inferred that the electron-transfer rate is retarded by the poor donor–acceptor electronic coupling, due to the scarce overlap between the ruthenium and cobalt t_{2g}/e_g orbitals.⁵³ An analogy between solution studies and DSSCs operational mechanism can thus be outlined, whereby the regeneration of the oxidized Ru(III) dye by Co(II) is expected to proceed through a mechanism similar to that occurring in solution, with the difference that the dye is anchored on the TiO_2 surface and only the cobalt complex can diffuse in the liquid electrolyte.

Motivated by the great interest in the full exploitation of the potential of cobalt-based electrolytes in the DSSCs framework, in this work we report a combined experimental and computational investigation to understand the nature of the interactions between the cobalt mediator and the dye-sensitized TiO_2 interface. We initially focus our attention on a series of Ru(II) dyes, to understand the reasons underlying the dramatic loss of efficiency observed for N719 in conjunction with cobalt electrolytes and to theoretically analyze the electron-transfer mechanism characterizing the dye regeneration process. We then extend the same concepts to a series of tailored organic dyes, D9L6, D21L6, and D25L6 (see Scheme 4), for which we report a high efficiency of 6.5% with a cobalt-based electrolyte. Finally, a series of different Co(II)/Co(III) complexes is

investigated to trace possible structure/property guidelines for the design of higher performance cobalt-based electrolytes.

2. METHODS, MODELS, AND EXPERIMENTAL DETAILS

2.1. Computational Details.

Periodic DFT calculations have been carried out within the generalized gradient approximation (GGA) using the PBE exchange–correlation functional.⁵⁸ The Car–Parrinello (CP) code as implemented in Quantum-Espresso package was used.⁵⁹ Electron-ion interactions were described by ultrasoft pseudopotentials with electrons from S 3s, 3p; O, N, and C 2s, 2p; H 1s; Ti 3s, 3p, 3d, 4s; Ru 4d, 5s, 5p; Co 4s, 5s, 4p, 5p 3d, 4d shells explicitly included in the calculations. Plane-wave basis set cutoffs for the smooth part of the wave functions and the augmented density were 25 and 200 Ry, respectively. The TiO_2 anatase (101) surface was modeled as a periodic slab of dimensions $20.48 \text{ \AA} \times 30.28 \text{ \AA}$ with a thickness of $\sim 7 \text{ \AA}$, containing 128 TiO_2 units. As shown in ref 60, the computed binding energies are almost independent of the number of layers in the anatase slabs.⁶⁰ The N719 dye was adsorbed on one side of the slab and the $[\text{Co}(\text{bpy})_3]^{3+}$ complex was initially placed above the dye with a distance Ru–Co of $\sim 15 \text{ \AA}$. A minimum separation between repeated images of $\sim 7 \text{ \AA}$ was ensured throughout the simulation. CP molecular dynamics (MD) simulations have been carried out, with an integration time step of 10 au, for a total simulation time of ca. 9 ps. The fictitious mass used for the electronic degrees of freedom is 1000 au, and we set the atomic masses to the value of 5 amu.

Electronic and energetic analysis on the ion-pairs and isolated molecules have been performed using the Gaussian 09 program package⁶¹ with B3LYP exchange–correlation functional.⁶² Solvation effects are evaluated by the conductor-like polarizable continuum model (C-PCM),⁶³ using acetonitrile as a solvent. A calibration study of the electronic and electrochemical properties of the $[\text{Co}(\text{bpy})_3]^{2+/3+}$ complexes has been carried out, along with comparative tests using 6-311G* and LANL2DZ basis sets.^{64,65} Geometry optimizations of the ion-pairs and isolated dyes have been carried out in solution with the LANL2DZ basis set, along with the corresponding pseudopotential for Ru and Co atoms. We also performed a comparative test using the B3LYP functional with a reduced amount of Hartree–Fock exchange (15%), hereafter B3LYP*.⁶⁶ Oxidation potentials are calculated both as solution energy differences and as Gibbs free energy differences (ΔE_{OX} and ΔG_{OX} in Table 1, respectively), the latter obtained by evaluating thermal contributions to the Gibbs free energy in vacuo.

Table 1. Oxidation Potentials (eV vs Vacuum) and High-Spin/Low-Spin Energy Difference (eV) Calculated at Different Levels of Theory

	B3LYP				B3LYP*	expt
	6-311G*		LANL2DZ		LANL2DZ	
	ΔE_{OX}	ΔG_{OX}	ΔE_{OX}	ΔG_{OX}	ΔE_{OX}	
$^2[\text{Co}(\text{bpy})_3]^{2+}$	4.88	5.04	4.79	5.00	4.57	5.00 ^a
$^4[\text{Co}(\text{bpy})_3]^{2+}$	5.06	5.37	4.96	5.27	4.59	
	HS/LS Splitting					
$\Delta E(^2\text{Co(II)} - ^4\text{Co(II)})$	0.18	0.33	0.17	0.27	0.02	<0.1 ^b
$\Delta E(^3\text{Co(III)} - ^1\text{Co(III)})$			1.33			1.7 ^c

^aExperimental value +4.44 from ref 25. ^bFrom ref 41a. and 42. ^cFrom ref 68.

The calculated ΔG_{OX} values can be directly compared to oxidation potentials determined from electrochemical measurements, e.g., cyclic voltammetry.

2.2. Method Calibration. Considering the fundamental role of redox potentials offsets in DSSCs operational mechanism and the possible role of HS/LS energetics, we investigate here the performance of our computational methodology in describing the Co(II)/Co(III) properties. Previous studies performed for Ru(II) dyes have ascertained the accuracy of the employed computational setup to describe the spectro-electrochemical properties for such systems.^{40,67} The $[\text{Co}(\text{bpy})_3]^{2+}$ complex has been previously computationally investigated,⁴² and a theoretical and computational approach to the electron-transfer process involving metal complexes has been reported by Newton.⁴³ For the reduced Co(II) complex we simulated both the LS and HS species, characterized by doublet and quartet spin-multiplicity, respectively. Relevant occupied molecular orbitals for the $^2,^4[\text{Co}(\text{bpy})_3]^{2+}$ and for the $^1,^3[\text{Co}(\text{bpy})_3]^{3+}$ complexes are reported in the Supporting Information. As expected, while the $^4[\text{Co}(\text{bpy})_3]^{2+}$ species shows two almost degenerate unpaired e_g electrons, the $^2[\text{Co}(\text{bpy})_3]^{2+}$ species shows one e_g unpaired electron. In both the quartet and doublet states the e_g orbitals are the HOMOs. The singlet $[\text{Co}(\text{bpy})_3]^{3+}$ species shows a closed-shell occupation of the t_{2g} orbitals, with six electron in the HOMO-3, HOMO-4 and HOMO-5 orbitals; the triplet $^3[\text{Co}(\text{bpy})_3]^{3+}$ shows one unpaired e_g electron.

The free energy difference in solution between the oxidized and the reduced species was compared with the experimental oxidation potentials. Oxidation potentials measured against the NHE electrode were reported against the vacuum level set at -4.44 eV vs NHE. As reported in Table 1, the oxidation potential for $[\text{Co}(\text{bpy})_3]^{2+/3+}$ calculated at B3LYP/6-311G* and B3LYP/LANL2DZ levels of theory are in excellent agreement with the experimental value of 0.56 V vs NHE, i.e., 5.0 V vs vacuum.²⁵ The calculated HS/LS splittings are evaluated in a range between 0.17 and 0.33 eV, depending on the basis set, which are larger than the experimental estimate <0.1 eV.⁴¹ This discrepancy was already observed for HS/LS splitting in metallorganic complexes⁶⁶ and the reduction of the Hartree–Fock exchange to a value of 15% was proposed, within the B3LYP* functional, to better reproduce the experimental HS/LS splitting.⁶⁶ As a matter of fact, a comparative test on the $[\text{Co}(\text{bpy})_3]^{2+/3+}$ complexes with the B3LYP* functional provided almost isoenergetic HS and LS states (Table 1). However, the oxidation potential calculated using B3LYP* is underestimated by ca. 0.5 eV compared to the electrochemical measurements (Table 1). Since a proper reproduction of the electrolyte redox potential is needed to reproduce the energetics of the regeneration process, we adopt the B3LYP approach throughout, taking into account the possible rescaling of the HS/LS energy difference. Our calculations for the Co(III) species confirm a closed-shell d^6 electron configuration

2.3. Materials Synthesis. The synthetic details of all dyes coded N719,⁶⁹ Z907,⁷⁰ D9L6,⁷¹ D21L6,⁷² and D25L6⁷³ have been described in previous studies. The synthesis of $[\text{Co}(\text{bpy})_3]^{3+/2+}$ was performed

according to a previously reported procedure.³² The adduct between N719 and $[\text{Co}(\text{bpy})_3]^{3+}$ was obtained by direct reaction between the Ru(II) N719 complex and the tris-chelate complex of Co(III) by following the following procedure: 1.5 equiv of N719, equal to 62 mg (0.052 mM), was dissolved in 10 mL of methanol, giving a dark red solution. Under magnetic stirring and bland heating (about 50 °C), an acetonitrile solution of the Co(III) complex, containing 1 equiv, equal to 34 mg (0.035 mM), was added to such system. The resulting solution assumes a reddish-brown coloration and was stirred at reflux for 1 h (at about 70 °C). After that time, a black-dark brown precipitate was formed in the body of the solution that was collected by filtration and washed three times with an acetonitrile/methanol solution (1:1). The final obtained product was 35 mg with a yield of about 59%, if we assume that the formula of the complex is Ru_3Co_2 .

2.4. Solar Cell Fabrication and Characterization. The nanocrystalline TiO_2 pastes were prepared using a previously reported procedure.⁷⁴ The TiO_2 transparent electrodes composed of ~ 20 nm anatase on fluorine-doped thin oxide (FTO, Solar 4 mm thickness, 10 Ω/sq , Nippon Sheet Glass, Japan) conducting glass were controlled to be ~ 6 μm by the number of screen printing passes. The TiO_2 electrodes were immersed into a ~ 0.3 mM dye solution in 4-*tert*-butanol/acetonitrile mixture (1:1 v/v) for ruthenium complexes and in ethanol for metal-free organic dyes and kept for 15 h at room temperature. The iodine-based electrolyte, coded JH91, consists of 0.55 M 1,3-dimethylimidazolium iodide (DMII), 0.1 M LiI, 0.05 M iodine, and 0.2 M 4-*tert*-butylpyridine (TBP) in 15/85 (v/v) mixture of valeronitrile and acetonitrile. The cobalt-based electrolyte, coded JH180, consists of 0.22 M $[\text{Co}^{\text{II}}(\text{bpy})_3](\text{B}(\text{CN})_4)_2$, 0.05 M $[\text{Co}^{\text{III}}(\text{bpy})_3](\text{B}(\text{CN})_4)_3$, 0.1 M LiClO_4 , and 0.2 M TBP in acetonitrile. The dye-adsorbed TiO_2 electrode and thermally platinized counter electrode on FTO (TEC 15 Ω/sq , Pilkington) were assembled into a sealed sandwich-type cell with a gap of a hot-melt ionomer film, Surlyn (25 μm , Du-Pont), where an electrolyte is employed. For photovoltaic measurements of the DSSCs, the irradiation source was a 450 W xenon light source (Osram XBO 450, Germany) with a filter (Schott 113), whose power was regulated to the AM 1.5G solar standard by using a reference Si photodiode equipped with a color-matched filter (KG-3, Schott) in order to reduce the mismatch in the region of 350–750 nm between the simulated light and AM 1.5G to <4%. In order to reduce scattered light from the edge of the glass electrodes of the dyed TiO_2 layer, a light shading mask was used on the DSSCs, so the active area of DSSCs was fixed to 0.2 cm^2 .

2.5. Photovoltage Transient Measurements. Photovoltage transients were observed by using a pump pulse generated by four red light emitting diodes controlled by a fast solid-state switch with a white light bias. The pulse of red light with widths of 100 ms was incident on the photoanode side of the cell, and its intensity was controlled to keep a suitably low level to generate the exponential voltage decay where the charge recombination rate constants are obtained directly from the exponential decay rate.⁷⁵ A white bias light, also incident on the same side of the device, was supplied by white diodes. The photoinduced charge density as function of the white light bias intensity was obtained by charge extraction measurement where the stored charges under open-circuit conditions were extracted by placing the cell under short-circuit conditions.⁷⁶ Small perturbation transient photocurrent measurements were performed in a similar manner to the open-circuit voltage decay measurement.

2.6. Magnetic Susceptibility Measurements. Magnetic susceptibility measurements were carried out at 300 K with an applied magnetic field of 0.1 T on polycrystalline samples of the Co(II) compounds: $[\text{Co}(\text{bpy})_3](\text{PF}_6)_2$, $[\text{Co}(\text{phen})_3](\text{PF}_6)_2$, $[\text{Co}(\text{py-pz})_3](\text{PF}_6)_2$, and $[\text{Co}(\text{bpy-pz})_2](\text{PF}_6)_2$ and their corresponding Co(III) derivatives $[\text{Co}(\text{bpy})_3](\text{PF}_6)_3$, $[\text{Co}(\text{phen})_3](\text{PF}_6)_3$, $[\text{Co}(\text{py-pz})_3](\text{PF}_6)_3$, and $[\text{Co}(\text{bpy-pz})_2](\text{PF}_6)_3$ (with masses in the range 20–42 mg) with a Quantum Design MPMS-XL-5 SQUID magnetometer. For samples $[\text{Co}(\text{py-pz})_3](\text{PF}_6)_2$ and $[\text{Co}(\text{bpy-pz})_2](\text{PF}_6)_2$ the magnetic measurements were also performed in the temperature range from 300 to 2 K since, as far as we know, the structure and the magnetic properties of these two complexes have not been reported previously.

Isothermal magnetization were performed at 2 K for samples compounds $[\text{Co}(\text{py-pz})_3](\text{PF}_6)_2$ and $[\text{Co}(\text{bpy-pz})_2](\text{PF}_6)_2$ with magnetic fields in the range 0–5 T. The susceptibility data were corrected for the sample holder previously measured under the same conditions and for the diamagnetic contribution as deduced by using Pascal's constant tables.

2.7. NMR Measurements. ^1H NMR spectra were measured on a Bruker DRX 400 spectrometer at 298.0 ± 0.1 K. Referencing is relative to external 3-(trimethylsilyl)propanesulfonic acid using the peak of CH_3COCH_3 as an internal reference ($\delta\text{H} = 2.22$ ppm). D_2O was purchased from Cortec and used as received. In separated NMR tubes, dilute solutions of N719 and $[\text{Co}(\text{bpy})_3][\text{PF}_6]_3$ (about 0.5 mM) were prepared by dissolving the solids in D_2O and adding a small amount of CH_3COCH_3 as internal reference. In a successive experiment, solid N719 was added to a solution of $[\text{Co}(\text{bpy})_3][\text{PF}_6]_3$ prepared as above, directly in the NMR tube, thus ensuring a constant concentration of $[\text{Co}(\text{bpy})_3]^{3+}$.

3. RESULTS AND DISCUSSION

3.1. Photovoltaic Results. Table 2 summarizes photo-current–voltage characteristics of DSSCs with different

Table 2. Photovoltaic Characteristics of DSSCs for N719 and Z907 with a $\sim 6 \mu\text{m}$ Thick TiO_2 film

dye	electrolyte	J_{sc} (mA/cm ²)	V_{oc} (mV)	FF	PCE (%)
N719	iodine ^a	11.6	675	0.66	5.2
	cobalt ^a	3.03	578	0.66	1.1
	iodine ^b	16.8	758	0.63	8.0
	cobalt ^b	3.8	620	0.76	1.8
Z907	iodine ^a	11.1	666	0.71	5.3
	cobalt ^a	4.43	649	0.74	2.1
	iodine ^b	15.9	790	0.61	7.7
	cobalt ^b	14.0	744	0.62	6.5

^aThe iodine-based electrolyte (JH91) consists of 0.55 M DMII, 0.1 M LiI, 0.05 M I_2 , and 0.2 M TBP in 15/85 (v/v) mixture of valeronitrile and acetonitrile. The cobalt electrolyte (JH180) consists of 0.22 M $[\text{Co}^{\text{II}}(\text{bpy})_3](\text{B}(\text{CN})_4)_2$, 0.05 M $[\text{Co}^{\text{III}}(\text{bpy})_3](\text{B}(\text{CN})_4)_3$, 0.1 M LiClO_4 , and 0.2 M TBP in acetonitrile. ^bData from ref 29.

ruthenium dyes in conjunction with iodine- or cobalt-based electrolytes under 1 sun simulated sunlight (100 mW/cm²). The power conversion efficiency (η) was derived from the equation $\eta = J_{\text{sc}}V_{\text{oc}}\text{FF}/I_0$, where J_{sc} is the short circuit current density, V_{oc} is the open-circuit voltage, FF is the fill factor, and I_0 is the photon flux illuminating the solar cells. Short-circuit current densities of over 10 mA/cm² and open-circuit voltages over 650 mV were produced by both N719 and Z907 ruthenium dyes under the employed conditions, with the iodine-based electrolyte. On the other hand, the same dyes in conjunction with the cobalt electrolyte produced drastically lower performances. Notice that the cobalt- and iodine-based electrolytes contain the same amount of Li^+ , so that a meaningful comparison of their photovoltaic characteristics can be done. A $V_{\text{oc}} = 578$ mV was measured for DSSCs fabricated with the N719 dye and a cobalt-based electrolyte, almost 100 mV lower than the V_{oc} obtained with the iodine-based electrolyte. Relatively smaller drops, ~ 20 and ~ 50 mV, were obtained by Z907 solar cells, respectively. Similarly, considerable drops in J_{sc} were observed in all devices employing cobalt electrolyte compared to those with iodine-based electrolyte. Again, N719-based DSSCs showed the biggest drop in J_{sc} when employing a cobalt electrolyte, with an associated lowest performance. Higher efficiencies were reported for both N719 and Z907 DSSCs in ref 29 (see also

Table 2), due to the different employed TiO_2 film thickness and architecture and overall conditions.

The I – V characteristics of DSSCs employing the D9L6, D21L6, and D25L6 organic dyes are quite different from those found for the ruthenium complexes. The data in Table 3,

Table 3. Photovoltaic Characteristics of DSSCs for D9L6, D21L6, and D25L6 with a $\sim 6 \mu\text{m}$ Thick TiO_2 Film

dye	electrolyte ^a	J_{sc} (mA/cm ²)	V_{oc} (mV)	FF	PCE (%)
D9L6	iodine	11.6	640	0.71	5.30
	cobalt	10.7	688	0.72	5.32
D21L6	iodine	12.9	703	0.66	6.00
	cobalt	12.3	852	0.63	6.63
D25L6	iodine	11.2	706	0.67	5.30
	cobalt	10.8	854	0.63	5.51

^aThe iodide electrolyte (JH91) consists of 0.55 M DMII, 0.1 M LiI, 0.05 M I_2 , and 0.2 M TBP in 15/85 (v/v) mixture of valeronitrile and acetonitrile. A cobalt electrolyte (JH180) consists of 0.22 M $[\text{Co}^{\text{II}}(\text{bpy})_3](\text{B}(\text{CN})_4)_2$, 0.05 M $[\text{Co}^{\text{III}}(\text{bpy})_3](\text{B}(\text{CN})_4)_3$, 0.1 M LiClO_4 , and 0.2 M TBP in acetonitrile.

obtained by using the same conditions, e.g., TiO_2 film thickness, as for the ruthenium dyes in Table 2, show that the organic dyes with cobalt electrolyte all exhibit slightly higher performances than with the iodine-based electrolyte. The reason for the improved performance of the organic dyes with cobalt electrolytes is mainly the higher V_{oc} . A ~ 50 mV V_{oc} increase is observed for D9L6, while a ~ 150 mV V_{oc} increase is measured for D21L6 and D25L6. Notably, the D21L6 and D25L6 dyes, featuring long alkoxy chains on the donor moiety, provided considerably high V_{oc} , as found for the D35 dye by Feldt et al.,²⁵ due to the more positive oxidation potential of the cobalt electrolyte compared to the iodine-based redox shuttle.

To provide a rationale for the origin of the V_{oc} differences observed when employing cobalt- and iodine based electrolytes, photovoltage transients were measured (Figure 1). Both N719- and Z907-based DSSCs show an increased lifetime in the iodine-based electrolyte. The difference is particularly striking for the N719 dye, which shows the shortest electron lifetimes with the cobalt- and the longest electron lifetimes with the iodine-based electrolyte, respectively. By contrast, the organic dyes D21L6 and D25L6, endowed with long alkoxy chains, show no significant change in the electron lifetime regardless of employed electrolyte. DSSCs based on the D9L6 dye, on the other hand, show much shorter electron lifetimes in conjunction with the cobalt electrolyte. Furthermore, at the matched electron density of 10^{17} , the Z907 ruthenium dye and the D9L6 organic dye show essentially the same electron lifetime (~ 10 ms) in the cobalt electrolyte, while N719 shows a factor ~ 5 shorter lifetime (see Figure 1). The trends of measured lifetimes are in agreement with the measured V_{oc} differences.

3.2. Dye/Cobalt Electrolyte Interactions. To provide a rationale for the observed trends in photovoltaic performances and electron lifetimes, with reference to the different behavior exhibited by the two ruthenium dyes and the set of organic dyes, we integrated our photovoltaic measurements with a detailed first principles computational analysis and by further experimental investigations. The main issues we wish to address here are (i) the possible role of ion-pairing between the ruthenium and organic dyes investigated experimentally and the cobalt electrolyte, as proposed in refs 24 and 30; (ii) the

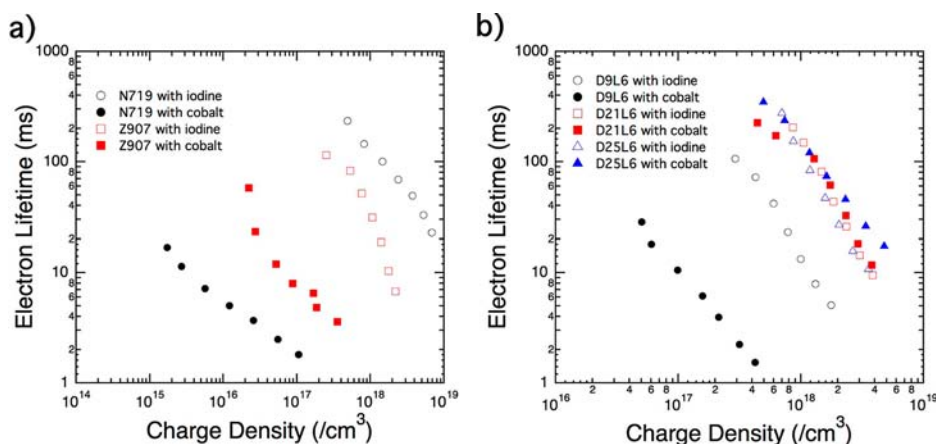


Figure 1. Electron lifetime as a function of photoinduced charge density. (a) DSSCs employing N719 (black markers) and Z907 (red markers) and (b) DSCs employing D9L6 (black markers), D21L6 (red markers), and D25L6 (blue markers). Open markers indicate results with iodine-based electrolyte, whereas closed markers indicate those with cobalt electrolyte.

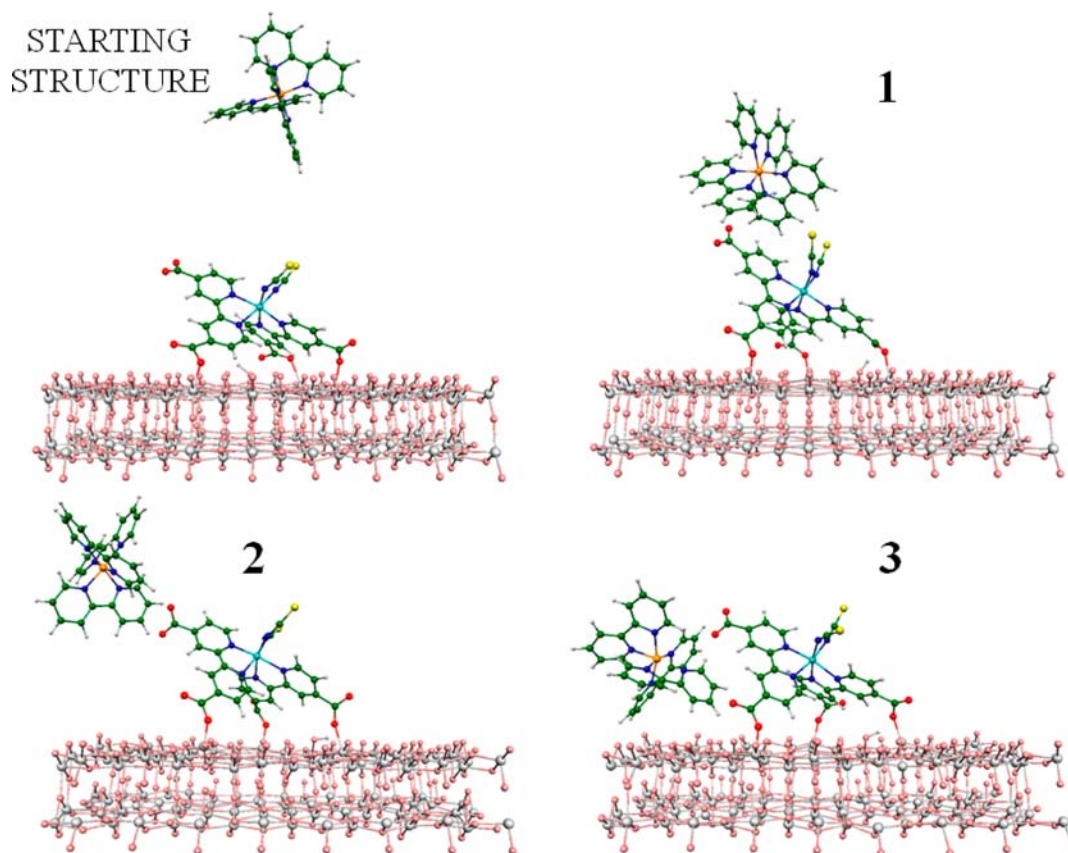


Figure 2. Representative geometrical structures for the N719(1H)³⁻@TiO₂/[Co(bpy)₃]³⁺ system extracted from the molecular dynamics simulation.

mechanism of regeneration of the oxidized dye, in relation to the possible role of the different cobalt spin states; and (iii) the effect of the Co(II)/Co(III) ligand environment and HS/LS equilibria in the oxidized dye regeneration kinetics. Understanding these aspects can lead to the independent optimization of new cobalt electrolytes with decreased recombination and increased regeneration kinetics.

To gain insight into the possible interactions occurring between the constituents of the cobalt electrolyte and the dye-sensitized TiO₂ interface, we carried out an *ab initio* MD

simulation, within the CP framework, of the N719 adsorbed onto the TiO₂ surface (N719@TiO₂) in the presence of the oxidized [Co(bpy)₃]³⁺ species. To maintain an overall charge neutrality in the simulation cell, we considered the N719 dye carrying one proton, N719(1H)³⁻, for which we reported an efficiency exceeding 11%.⁸ This model is obviously limited, lacking of solvent molecules and/or of compensating counterions. We mention, however, that the N719 dye is known to be mainly present as a negatively charged species both in solution³⁸ and upon adsorption onto TiO₂;³⁹ Co(III)–

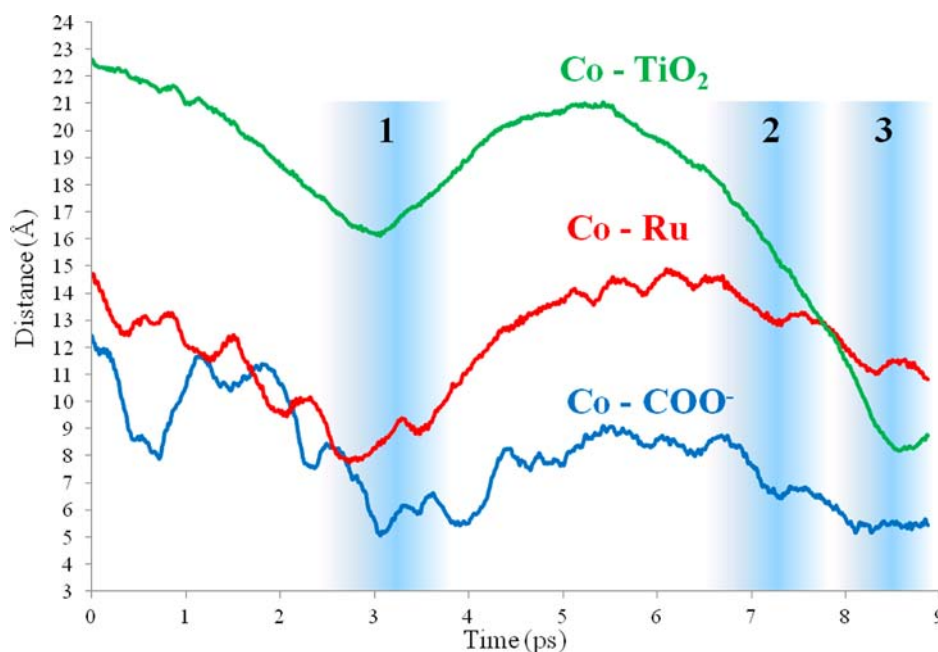


Figure 3. Dynamical evolution of the distances between the Co and the Ru atoms, the Co atom and the TiO₂ surface, and Co atom and the carboxylate group of the N719(1H).

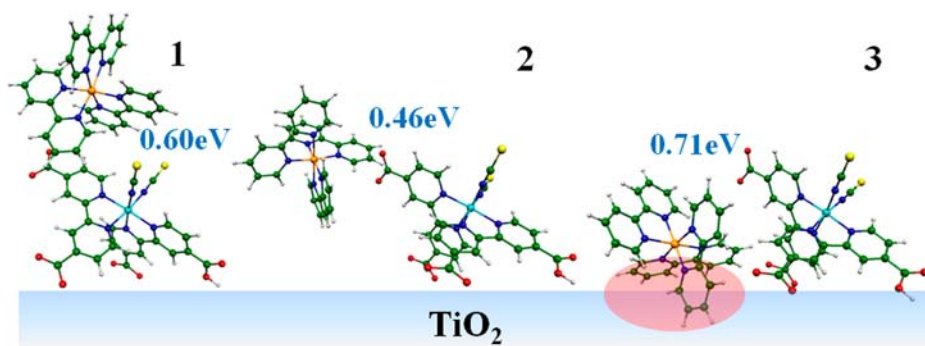


Figure 4. Binding energies of the optimized three structures selected from the dynamics simulation.

hexamine complexes are mostly present in solution as dicationic species, with one counterion.^{77,78} Under these circumstances, our dynamics simulation should be taken as a means to explore the potential energy landscape of the dye-sensitized TiO₂ in the presence of the electrolyte, rather than a precise tool to assess the properties of the real system. A more realistic picture of the interactions between the dyes and the electrolyte components, including both solvent and counterion effects, is presented below.

We start our simulation from the N719 dye anchored to the TiO₂ slab with three carboxylate groups, as reported in our previous theoretical works.^{40,79} Recent X-ray reflectometry data lend support to this anchoring mode.⁸⁰ From this optimized geometry, we added the [Co(bpy)₃]³⁺ complex ca. 15 Å above the dye; the entire system, N719(1H)³⁻@TiO₂/[Co(bpy)₃]³⁺, was locally optimized, providing the starting structure of Figure 2. From this geometry we thermalized the systems at 350 K for 2 ps, keeping fixed the N719(1H)³⁻-Co(bpy)₃³⁺ distance at its initial value, and then we performed an unconstrained MD simulation for a total time of 9 ps (see the movie file in Supporting Information).

In Figure 3 we report the evolution of the representative atomic distances as a function of the simulation time. The

cobalt–ruthenium distance (Co–Ru in Figure 3), roughly representing the dye/electrolyte interaction, decreases from its ~15 Å initial value to ~8 Å within the first 3 ps of simulation. The distance between the cobalt complex and the TiO₂ surface (Co–TiO₂ in Figure 3) shows a similar decrease, suggesting a spontaneous approaching of the [Co(bpy)₃]³⁺ species toward the surface-adsorbed dye and consequentially toward the TiO₂ semiconductor. Moreover, a crucial role is played by the dye carboxylate group not bound to the TiO₂ surface, which effectively attracts the positively charged cobalt complex. Indeed the distance between the cobalt and the –COO⁻ group (Co–COO in Figure 3) decreases during the simulation approaching a value of ~5 Å. The overall picture extracted from our dynamics simulation underlines the formation of an associated complex between the cobalt electrolyte and the TiO₂-adsorbed dye. The driving force of this association is clearly the electrostatic attraction between the positively charged [Co(bpy)₃]³⁺ and the adsorbed negatively charged N719(1H)³⁻@TiO₂ system. It is also interesting to notice that, toward the end of the simulation, [Co(bpy)₃]³⁺ contacts the TiO₂ surface, as signaled by a Co–TiO₂ distance which is shorter than the Ru–TiO₂ distance.

Table 4. Binding Energy (eV) of the Ion-Pairs for All Investigated Dyes with the Cobalt Electrolyte at Their Different Spin-Multiplicity^a

dye	charge	Ru(II)								Ru(III)	
		Co(III)				⁴ Co(II)				⁴ Co(II)	² Co(II)
N719(1H)	-3	0.60	0.42	0.28	0.16	0.36	0.36	0.25	0.17	0.23	0.20
N719(2H)	-2	0.40	0.22	0.07	-0.05	0.29	0.29	0.18	0.10	0.18	0.19
Z907(0H)	-2	0.38	0.19	0.05	-0.07		0.27	0.16	0.08	0.14	0.10
Z907(1H)	-1	0.28	0.10	-0.05	-0.17		0.21	0.10	0.03		0.06
Z907(2H)	0	0.20	0.01	-0.13	-0.25		0.15	0.04	-0.04	0.02	0.00
no. of counterions		0	1	2	3	0	0	1	2	0	0

^aFor the Ru(II)/Co(III) and Ru(II)/Co(II) ion-pairs the binding energy as a function of the number of B(CN)₄⁻ counterions is also reported. The binding energies are defined as $E[\text{Ru}\cdots\text{Co}] + nE[\text{B}(\text{CN})_4^-] - E(\text{Ru}) - E[(\text{Co})][\text{B}(\text{CN})_4^-]_n$.

From the dynamics simulation we extracted three representative structures (1, 2, and 3 in Figure 2) located ca. 3.2, 7.2, and 8.6 ps along the simulated trajectory, which have been employed as starting structures for a subsequent geometry optimization in solution. Notice that the dye remains anchored by three carboxylic groups throughout the dynamics simulation, suggesting that this binding mode is effectively stable. Structure 1 is characterized by the specific interaction between the [Co(bpy)₃]³⁺ complex and the unbound carboxylate group and the NCS⁻ ligands of the N719 dye. Structure 2 shows one specific interaction between the cobalt complex and the unbound carboxylate, while structure 3 is characterized by the cobalt complex placed close to the TiO₂ while it is interacting with the free carboxylate group and with a carboxylic oxygen of one anchoring carboxylate group of the dye, Figure 2.

To evaluate the strength of the N719(1H)³⁻⋯[Co(bpy)₃]³⁺ interaction in the typical electrolyte solution environment, we optimized structures 1, 2, and 3 after removal of the TiO₂ slab in acetonitrile solution (B3LYP/LANL2DZ/CPCM). The optimized geometries and the calculated binding energies, obtained by energy difference with the isolated N719(1H)³⁻ and [Co(bpy)₃]³⁺ species, are shown in Figure 4, and underline the effective formation of an ion-pair characterized by high solution binding energies values, varying in the range 0.46–0.71 eV for the three investigated structures. The highest binding energy (0.71 eV) is associated with structure 3, where the cobalt complex interacts with three dye carboxylate groups. Notice, however, that this type of interaction is probably less likely to occur when the dye is anchored as a packed monolayer to the TiO₂ surface. We therefore focused our attention on the second more stable structure 1, only 0.11 eV less stable than 3, and we separately investigated the effect of dye protonation and number of B(CN)₄⁻ counterions binding the [Co(bpy)₃]³⁺ species, on the calculated binding energies (see Supporting Information for optimized geometries of [Co(bpy)₃]^{2+/3+}[B(CN)₄]⁻_n, n = 1–3). As shown in Table 4, by reducing the negative charge of the dye, moving from N719(1H)³⁻ to N719(2H)²⁻, we find a decrease of the binding energy of 0.20 eV associated to the reduction of the electrostatic attraction between the two fragments. Based on structure 1, we also investigated the energetics of ion-pair formation for Z907 as a function of the number of dye protons (from 0 to 2; see Table 4 and Supporting Information).

By looking at the data for the Ru(II)–Co(III) adducts reported in Table 4, the binding energies for the ruthenium dyes of the same total charge are similar (0.40 and 0.38 eV for N719(2H) and Z907(0H), respectively). As expected, the binding energy varies with the total dye charge, from 0.40 eV

for N719(2H) to 0.20 eV for the neutral Z907(2H). Since these are the species which are used to dye the TiO₂ films in DSSCs, a lower probability of intercepting TiO₂ – injected electrons is predicted for Z907 with respect to N719, as previously suggested.²⁹ Notably, for all the investigated (neutral) organic dyes we calculate almost zero binding energies with [Co(bpy)₃]³⁺ (see optimized structures and binding energies in Supporting Information), while for the neutral Z907(2H) a binding energy of 0.20 eV is calculated. By calculating the Mulliken charge on the S atoms of the Z907(2H) dye NCS groups, we obtain a value of -0.39 electrons, which underlines the possible role of the anionic NCS⁻ ligands of the ruthenium dyes in the ion-pair formation with the cobalt electrolyte. As it could be anticipated, the presence of B(CN)₄⁻ counterions in the cobalt complexes reduces the binding energy of the former with the ruthenium dye. Notably, for the N719 dye the calculated binding energies are always positive, i.e., the ensuing Ru(II)/Co(III) ion-pair is more stable than the starting reagents, for all the possible combinations of protons/counterions except N719(2H)/Co(III)[B(CN)₄]⁻₃. A similar trend is calculated for Z907, although lower binding energies are computed in this case. As mentioned above, Co(III)–hexamine complexes are mainly found as dicationic species in solution, i.e., with one compensating counterion.^{77,78}

To probe experimentally the existence of the proposed Ru(II)–Co(III) interaction, we synthesized the product corresponding to the ionic exchange reaction between the N719-TBA₂ dye and the [Co(bpy)₃][PF₆]₃ species. The two reagents were mixed in a 1:1 methanol/acetonitrile solution, in a 3:2 ratio, which would correspond to formation of the neutral (N719)₃-[Co(bpy)₃]₂ salt. A dark powder was obtained in 59% yield, which after repeated washing in the same methanol/acetonitrile solution used for the synthesis, was subjected to NMR analysis. The powder was not soluble in either methanol or acetonitrile, but was moderately soluble in water. NMR analysis of the powder in D₂O confirmed the presence of both N719 and [Co(bpy)₃]³⁺. Although we were not able to determine the precise stoichiometry of the salt, this data is indicative of the tendency of N719 and Co(III) ions to form strong ionic interactions in a solution environment quite similar to that employed in the electrolyte formulations. Applying the same procedure to the Z907 dye under identical conditions, no precipitate was observed.

To further probe the possible interaction between N719 and [Co(bpy)₃]³⁺, additional NMR experiments were performed. Addition of solid N719 to a dilute solution of [Co(bpy)₃]-[PF₆]₃ in D₂O causes a low-frequency frequency shift for all the

aromatic ^1H NMR resonances of the $[\text{Co}(\text{bpy})_3]^{3+}$ species (Figure 5 and Supporting Information). Comparison with the

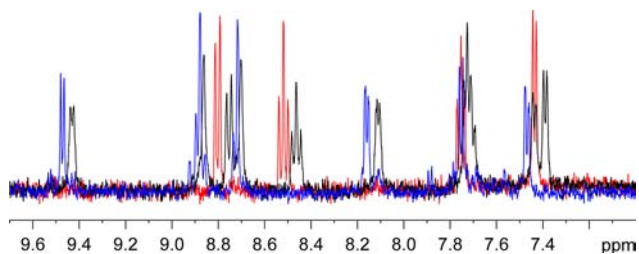
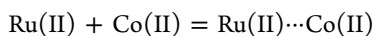


Figure 5. Section of the aromatic region of the ^1H NMR spectra of $[\text{Co}(\text{bpy})_3][\text{PF}_6]_3$ (red trace), N719 (blue trace), and $[\text{Co}(\text{bpy})_3][\text{PF}_6]_3$ plus N719 (black trace) in D_2O at 298 K.

NMR spectrum of an N719 sample obtained under identical experimental conditions, indicate that all the aromatic ^1H NMR resonances of the dye are also low-frequency shifted in the presence of $[\text{Co}(\text{bpy})_3][\text{PF}_6]_3$. Notably, for both the metal cation and the metal anion, chemical shift variations are different for different resonances. These observations are consistent with the formation of new ionic aggregates; the observed low-frequency shifts are typical of stacking interactions between aromatic rings and strongly suggest a close proximity between the aromatic moieties of N719 and $[\text{Co}(\text{bpy})_3]^{3+}$.⁸¹

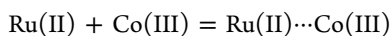
Our combined calculated binding energy values and experimental observations are consistent with the photovoltaic performances and lifetimes measured for the investigated compounds, with Z907 showing longer lifetimes (and better performances) than N719, reflecting the stronger interaction between N719 and $[\text{Co}(\text{bpy})_3]^{3+}$. The investigated organic dyes deliver higher efficiency with cobalt electrolytes because of their calculated low binding energy with $[\text{Co}(\text{bpy})_3]^{3+}$, which leads to a reduced recombination process by virtue of a decreased Co(III) approach to the TiO_2 surface. This effect is found to be increased by adding bulky alkyl chains to the dye donor moiety, which work as a further insulator between the TiO_2 electrons and the oxidized species in the electrolyte.^{29,34}

The calculated binding energies of the $\text{Ru}(\text{II})\cdots\text{Co}(\text{II})$ complexes, also reported in Table 4, can be used to estimate the competition between the Co(II) and Co(III) complexes in approaching the dye-sensitized semiconductor surface. For the N719 dye, we calculated both $^4\text{Co}(\text{II})\cdots\text{Ru}(\text{II})$ and $^2\text{Co}(\text{II})\cdots\text{Ru}(\text{II})$ species, obtaining the same binding energy (see Table 4), which are $\sim 0.1\text{--}0.2$ eV lower than the corresponding values calculated for the $\text{Ru}(\text{II})\cdots\text{Co}(\text{III})$ system, depending on the degree of dye protonation. In DSSCs, however, the concentration of Co(II) is usually 10 times higher than that of the Co(III) species. Considering the two competitive reactions between the Co(II)/Co(III) complexes in solution and the TiO_2 -adsorbed Ru(II) dye, indicated by the ADS subscript, we can express their equilibrium constants as



$$K^{\text{II}} = [\text{Ru}(\text{II})\cdots\text{Co}(\text{II})]_{\text{ADS}} / [\text{Co}(\text{II})][\text{Ru}(\text{II})]_{\text{ADS}}$$

and

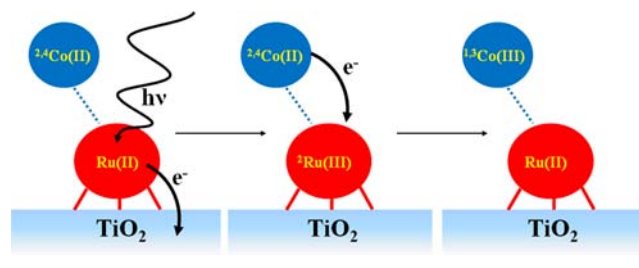


$$K^{\text{III}} = [\text{Ru}(\text{II})\cdots\text{Co}(\text{III})]_{\text{ADS}} / [\text{Co}(\text{III})][\text{Ru}(\text{II})]_{\text{ADS}}$$

We can now use the calculated binding energies for determining the $K^{\text{II}}/K^{\text{III}}$ ratio and thus for evaluating the $[\text{Ru}(\text{II})\cdots\text{Co}(\text{II})]_{\text{ADS}}/[\text{Ru}(\text{II})\cdots\text{Co}(\text{III})]_{\text{ADS}}$ ratio, assuming that the initial $[\text{Ru}(\text{II})]_{\text{ADS}}$ concentration is the same, which is perfectly reasonable for DSSCs fabricated under comparable conditions with the same dye, and setting the initial concentrations of Co(II) and Co(III) to 0.2 and 0.02 M, respectively, as in the most typical experimental conditions, and to 0.22 and 0.05 M as in our experimental setup. To assess the impact of counterions in determining this equilibrium, we evaluate the $[\text{Ru}(\text{II})\cdots\text{Co}(\text{II})]/[\text{Ru}(\text{II})\cdots\text{Co}(\text{III})]$ ratio for the case with no counterions and for the case of two counterions for both Co(II) and Co(III) complexes. For the naked $[\text{Co}(\text{bpy})_3]^{2+/3+}$ species we obtain a value of $[\text{Ru}(\text{II})\cdots\text{Co}(\text{II})]/[\text{Ru}(\text{II})\cdots\text{Co}(\text{III})] = 0.14\text{--}0.06$ for N719(2H), which increases to 1.41–0.62 for Z907(2H), depending on the electrolyte composition. For the case with two counterions, we find values of the $[\text{Ru}(\text{II})\cdots\text{Co}(\text{II})]/[\text{Ru}(\text{II})\cdots\text{Co}(\text{III})]$ ratio of 32.3 and 337.1 for N719(2H) and Z907(2H), respectively. Thus, based on calculated binding energies for the same number of counterions (0 or 2) carried by the Co(II)/Co(III) complexes, the $\text{Ru}(\text{II})\cdots\text{Co}(\text{III})$ ion-pair is always 10 times favored for N719(2H) compared to Z907(2H), despite the decreased tendency to form ion pairs when considering two counterions. The picture extracted from our calculations suggest therefore that a higher probability of recombination with TiO_2 – injected electrons is to be expected for N719 compared to Z907. This is perfectly in line with our lifetime measurements and with the reported photovoltaic efficiencies.²⁹ We also notice that the binding energies of the $^2\text{Ru}(\text{III})\cdots^4\text{Co}(\text{II})$ and $^2\text{Ru}(\text{III})\cdots^2\text{Co}(\text{II})$ (Table 4) are similar and also in this case are related to the degree of the dye protonation, suggesting a minor role of the Co(II) spin state on the ion-pair binding energies.

3.3. Dye Regeneration Mechanism. The oxidized dye regeneration mechanism corresponds to the electron-transfer process from Co(II) to Ru(III) to give the Co(III) and Ru(II) products (see Scheme 5). As it was mentioned in the

Scheme 5. Schematic Representation of the Steps Involved in the Dye Regeneration Mechanism, Following Light Absorption and Electron Injection

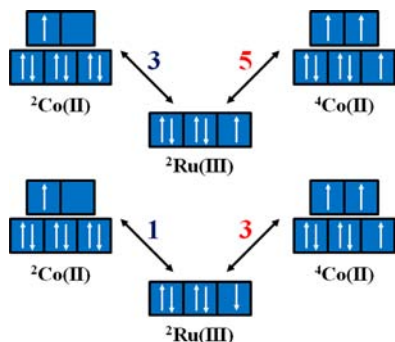


Introduction, solution studies suggested a much faster electron transfer to Ru(III) dyes from Co(II) ions in the LS state rather than in the HS state.^{50,51} The smaller reorganization for the LS pathway was suggested to be responsible for the faster electron transfer compared to the HS pathway.^{50,51,57}

Having calculated the structures of the interacting complexes, we simulate here the possible Co(II)–Ru(III) couples formed after injection of one electron from the dye excited state to TiO_2 : (i) the $^2\text{Co}(\text{II})\text{--}^2\text{Ru}(\text{III})$ couple, with one unpaired electron on the $^2\text{Co}(\text{II})$ and one on the $^2\text{Ru}(\text{III})$ centers; and (ii) the $^4\text{Co}(\text{II})\text{--}^2\text{Ru}(\text{III})$ species, with three unpaired electrons

on $^4\text{Co(II)}$ and one on the $^2\text{Ru(III)}$ center. Two spin states are accessible for each couple, depending on the ferro- or anti-ferromagnetic coupling between $^2/4\text{Co(II)}$ and $^2\text{Ru(III)}$ (see Scheme 6), i.e., a diradical singlet or triplet for $^2\text{Co(II)}-^2\text{Ru(III)}$

Scheme 6. Possible Coupling Patterns between $^2\text{Co(II)}$, (left), $^4\text{Co(II)}$ (right), and $^2\text{Ru(III)}$ (middle)^a



^aFor $^4\text{Co(II)}-^2\text{Ru(III)}$ both triplet and quintet spin states are possible, while for $^2\text{Co(II)}-^2\text{Ru(III)}$ triplet and singlet spin states are possible.

(III) and a triplet or a quintet for $^4\text{Co(II)}-^2\text{Ru(III)}$. The final product of the dye regeneration process, $\text{Co(III)}-\text{Ru(II)}$, can be either a closed-shell singlet or a triplet species, depending from the local spin on the Co(III) ion.

As reported in the literature,^{57,68} the triplet $[\text{}^3\text{Co}(\text{bpy})_3]^{3+}$ species is 1.7 eV higher than the singlet $[\text{}^1\text{Co}(\text{bpy})_3]^{3+}$ species, suggesting that the final product of the reaction is reasonably the $\text{Co(III)}\cdots\text{Ru(II)}$ closed-shell singlet and that the reaction pathway leading to the $^3\text{Co(III)}$ species is disfavored. The $^4\text{Co(II)}-^2\text{Ru(III)}$ HS species is calculated ~ 0.2 eV below the $^2\text{Co(II)}-^2\text{Ru(III)}$ LS species, similar to what found for the isolated Co(II) complex, suggesting a negligible electronic interaction between the Co(II) and Ru(III) ions. This is confirmed by the isoenergetic $^4\text{Co(II)}-^2\text{Ru(III)}$ species with ferro- (quintet) or anti-ferromagnetic (triplet) coupling (Scheme 6). In the following we thus limited our attention to the HS quintet $^4\text{Co(II)}-^2\text{Ru(III)}$ and to the LS triplet $^2\text{Co(II)}-^2\text{Ru(III)}$ cases. Considering the calibration study performed on the single Co(II) complexes, we set to zero the energy difference between the HS and LS states from now on, to recover the systematic error introduced by the B3LYP functional in the HS/LS splitting.

We then evaluate the electron-transfer (EL) parameters of dye regeneration following the Marcus equation:⁴⁴

$$k_{\text{et}} = \frac{2\pi}{\hbar} |H_{\text{AB}}|^2 \frac{1}{\sqrt{4\pi\lambda k_{\text{B}}T}} e^{-\frac{(\lambda + \Delta G^0)^2}{4\lambda k_{\text{B}}T}} \quad (1)$$

where H_{AB} is the electronic coupling, λ is the reorganization energy, and ΔG^0 is the free energy difference between the products and reagents. The activation energy of the electron-transfer process is accordingly defined as $\Delta G^* = (\lambda + \Delta G^0)^2 / 4\lambda$. We start our analysis from the $\text{Ru(III)}\cdots\text{Co(II)}$ system: considering N719(1H), with three negative charges, we calculate a 0.23/0.20 eV binding energy with $[\text{Co}(\text{bpy})_3]^{2+}$ for the HS/LS cases (Table 4), respectively, which is comparable to the value of ~ 0.1 eV estimated in ref 57. from the ratio of the kinetic rate constants of association and

dissociation in solution for the $[\text{Ru}(\text{dcbpy})_3]^{3-}\cdots[\text{Co}(\text{bpy})_3]^{2+}$ ion-pair ($\text{dcbpy} = 2,2'$ -bipyridine-4,4'-dicarboxylate).⁵⁷

We then calculated the reorganization energies and the thermodynamics for the regeneration reaction considering both HS and LS $\text{Co(II)}-\text{Ru(III)}$ interacting species. The results for the N719(1H), N719(2H), and Z907(0H) cases are reported in Figure 6.

The reorganization energy (λ) has been calculated as the difference between the single-point energy in solution of the reagent at the geometry of the product and the ground-state energy of the reagent (see Figure 6), using equilibrium solvation. It can be noticed that the reorganization energies associated with the HS and LS cases, $^{\text{HS}}\lambda$ and $^{\text{LS}}\lambda$, are substantially different: $^{\text{HS}}\lambda$ values in the range 1.36–1.45 eV are calculated, depending on the nature of the dye and its protonation state, to be compared to $^{\text{LS}}\lambda$ values in the range 0.61–0.72 eV. The calculated reorganization energies for the associated complexes are almost identical to those calculated for the doublet and quartet states of the isolated $[\text{Co}(\text{bpy})_3]^{2+}$ complex, 0.63 and 1.36 eV, respectively. Notice, that using non-equilibrium solvation a rigid 0.72 (0.54) eV up-shift is calculated for both HS and LS reorganization energies of the isolated (interacting) complex. As a matter of fact, the calculated λ values for the isolated dyes (Supporting Information) are much lower than those of the cobalt complexes, being all ~ 0.1 eV for both organic and metal-organic systems. Thus the calculated λ values for the associated complexes are roughly equal to the sum of the λ values of the separated dyes and cobalt complex, suggesting a minimal electronic communication between the interacting species, beyond their electrostatic interaction.

The calculated values for ΔG^0 , i.e., the free energy difference between the products and reagents, are also reported in Figure 6. We recall that, on the basis of our calibration study, we have simply set to zero the energy difference between the HS and LS states of $[\text{Co}(\text{bpy})_3]^{2+}$. As one can notice, a 0.44 eV regeneration driving force is calculated for both N719(1H) and N719(2H), while this value is reduced to 0.24 eV for Z907(0H). The calculated values are in excellent agreement with the reported oxidation potential differences between N719 and Z907 dyes and $[\text{Co}(\text{bpy})_3]^{2+}$ of 0.52 and 0.37 V, respectively.²⁹ Notice that since we have set the HS and LS species to be isoenergetic and since the reaction proceeds to the same products, the same ΔG^0 is calculated for both the HS and LS pathways. Thus, lower activation energies for all dyes are associated with the LS pathway by virtue of the lower reorganization energies. This result is in line with previously experimental work⁵⁷ in which the rate of electron transfer from the HS Co(II) $[\text{Co}(\text{bpy})_3]^{2+}$ complex to the Ru(III) $[\text{Ru}(\text{dcbpy})_3]^{3-}$ species was found to be slower than the electron transfer from the LS Co(II) $[\text{Co}(\text{tpy})_2]^{2+}$ complex to the same Ru(III) species. The increased electron-transfer rate was ascribed to the lower inner-sphere reorganization energy of the LS $[\text{Co}(\text{tpy})_2]^{2+}$ species compared to the HS $[\text{Co}(\text{bpy})_3]^{2+}$ species.⁵⁷ Furthermore, our model predicts a lower activation energy for N719 compared to Z907, in agreement with the 5 times faster regeneration half-times measured for N719 (2 μs) with respect to Z907 (10 μs).²⁴ Taking the exponential of the computed activation energies for the N719(2H) and Z907(0H), we calculate a N719/Z907 regeneration rate ratio of 7.0, very close to the factor of 5 retrieved experimentally.²⁴ Notice that the λ values calculated for N719(2H) and Z907(0H) regeneration are similar (Figure

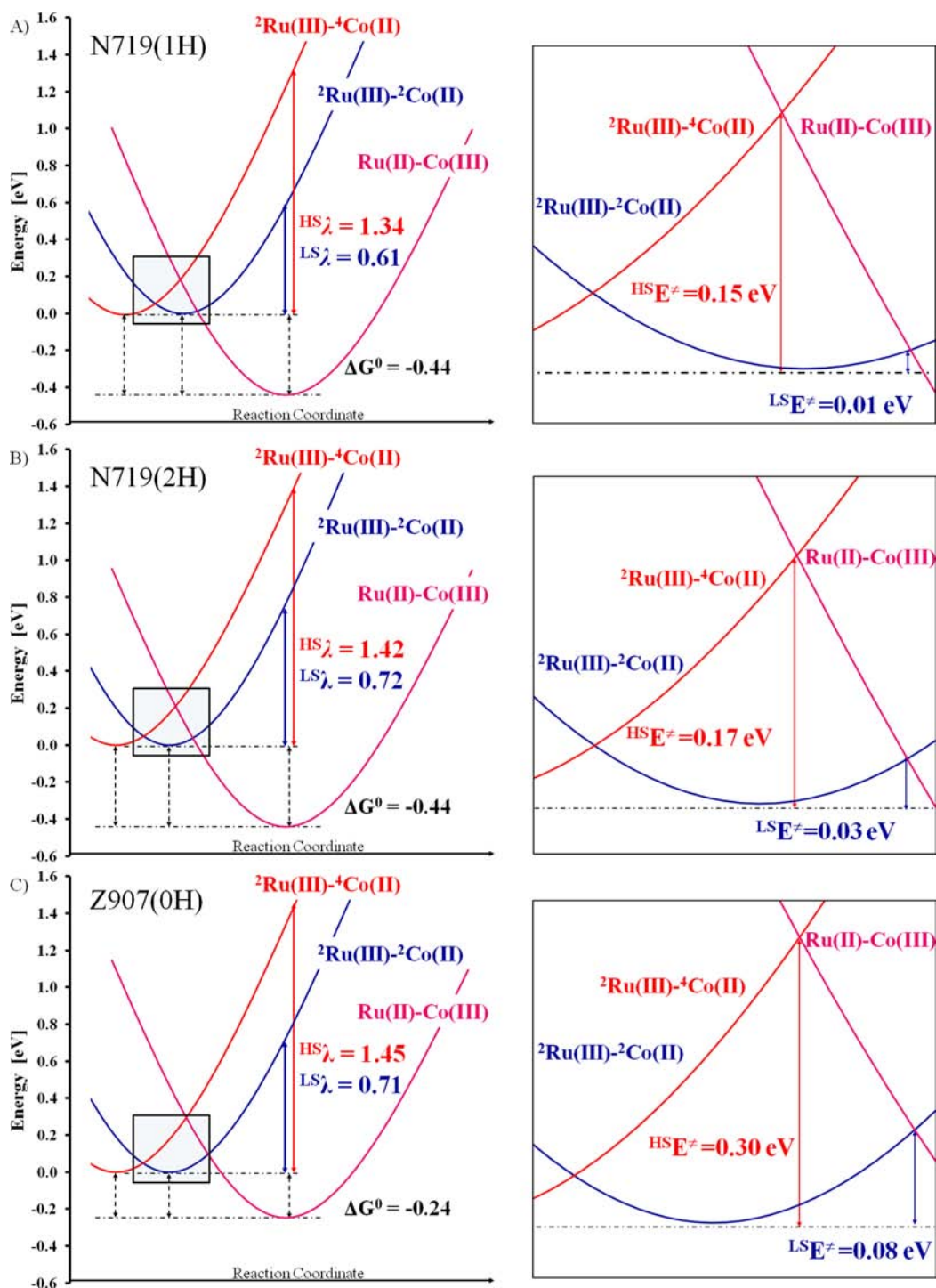


Figure 6. (A) Reaction profile of the regeneration process of N719(1H)³⁻ by [Co(bpy)₃]²⁺. (B) Reaction profile of the regeneration process of N719(2H)²⁻ by [Co(bpy)₃]²⁺. (C) Reaction profile of the regeneration process of Z907(0H)³⁻ by [Co(bpy)₃]²⁺. On the right-hand side of each panel, a zoom of the region highlighted on the left-hand sides is reported.

6B,C), so the lower activation energy calculated for the former is due to the more positive redox potential of N719, which leads to a more negative ΔG^0 of the electron transfer.

Overall, our results underline that the preferred dye regeneration pathway is the LS pathway, which is favored by the substantially lower reorganization energy. Similar arguments were proposed for model Co(II)→Ru(III) electron-transfer reactions in solution.⁵⁷ This also implies that the spin-crossover equilibrium between the ⁴Co(II) and the ²Co(II)

species and the rate of HS to LS conversion might be crucial to ensure a high concentration of the reactive LS species. Most notably, our calculated reorganization energies for the LS pathways (0.6–0.7 eV) are in excellent agreement with the average reorganization energy (0.8 ± 0.1 eV) recently reported by Feldt et al. for a series of cobalt complexes,³⁴ lending support to the proposed regeneration pathway.

On the basis of our calculated data, we can draw a schematic molecular orbital diagram of the injection/regeneration LS

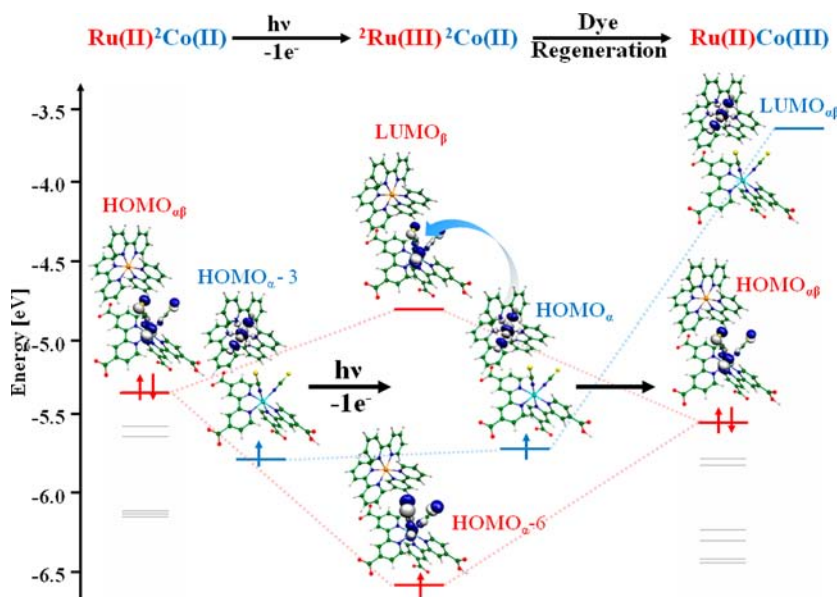


Figure 7. Injection/regeneration mechanism for N719(1H) with $[\text{Co}(\text{bpy})_3]^{2+}$ along the LS pathway. Red and blue labels refer to states maximally localized on the N719 dye and $[\text{Co}(\text{bpy})_3]^{2+/3+}$, respectively.

pathway for N719(1H) in Figure 7; see also Supporting Information for spin populations. Before light absorption, the ion-pair $\text{Ru}(\text{II})-\text{Co}(\text{II})$ has one unpaired e_g electron located on the ${}^2\text{Co}(\text{II})$ center (spin density 0.94 e). After electron injection, the oxidized dye shows one unpaired electron on the Ru–NCS orbital (spin density 0.70 e) and still one unpaired e_g electron on the ${}^2\text{Co}(\text{II})$ (spin density 0.94 e). Finally, the ${}^2\text{Co}(\text{II})$ unpaired electron is transferred to the unoccupied Ru(III) LUMO, regenerating the Ru(II) species and providing the Co(III) species (both as closed shells). It is also interesting to notice that, if the reaction were to proceed via a HS pathway that preserves the total spin, an excited Co(III) triplet state would be formed, which is very energetically unfavorable. Thus, the reaction would most likely proceed by a non-adiabatic pathway involving flipping of one spin along the reaction coordinate. This spin-crossing barrier would show up as a decrease of the electronic coupling term (H_{AB} in 1),⁴³ further contributing to a reduction of the overall HS regeneration rate. We may also notice that the formation of the intermediate $\text{Ru}(\text{III})\cdots\text{Co}(\text{II})$ ion pair is not strictly necessary to our discussion, and, to the best of our knowledge, this intermediate has not been identified so far. We notice, however, that a related intermediate species was spectroscopically characterized in Γ/I_3^- -based electrolytes.^{82,83}

Considering the potential importance of HS/LS energetics highlighted above, and in light of the results of ref 34 obtained for a series of cobalt complexes with different ligands, we systematically investigated the redox potential, HS/LS splitting, and reorganization energy by combining computational analyses and magnetic susceptibility measurements. We looked at the series of $[\text{Co}(\text{R-bpy})_3]^{2+/3+}$ (with two R substituent in 4,4' position, R = H, CH_3 , $\text{C}(\text{CH}_3)_3$, Cl); $[\text{Co}(\text{R-phen})_3]^{2+/3+}$ (phen = 1,10-phenanthroline, with R substituent in 5 position, R = H, Cl, NO_2); $[\text{Co}(\text{py-pz})_3]^{2+/3+}$ (py-pz = 6-(1H-pyrazol-1-yl)-2-pyridine); $[\text{Co}(\text{bpy-pz})_2]^{2+/3+}$ (bpy-pz = 6-(1H-pyrazol-1-yl)-2,2'-bipyridine); and $[\text{Co}(\text{tpy})_2]^{2+/3+}$ (tpy = terpyridine). The investigated complexes span a widely varying range of oxidation potentials and are representative of tris-bidentate

($[\text{Co}(\text{R-bpy})_3]^{2+/3+}$, $[\text{Co}(\text{py-pz})_3]^{2+/3+}$, and $[\text{Co}(\text{R-phen})_3]^{2+/3+}$) and bis-tridentate ($[\text{Co}(\text{bpy-pz})_2]^{2+/3+}$ and $[\text{Co}(\text{R-tpy})_2]^{2+/3+}$) types of complexes, allowing us to systematically investigate the impact of such variables on the HS/LS energy difference and reorganization energies.

The values of the product of the molar magnetic susceptibility per Co(II) ion at room temperature times the temperature ($\chi_m T$, proportional to the magnetic moment) are displayed in Table 5. All the investigated compounds contain

Table 5. $\chi_m T$ Product per Co(II) Ion at Room Temperature ($\text{cm}^3\cdot\text{K}\cdot\text{mol}^{-1}$) for the $[\text{Co}(\text{bpy})_3]^{2+}$, $[\text{Co}(\text{phen})_3]^{2+}$, $[\text{Co}(\text{bpy-pz})_2]^{2+}$, and $[\text{Co}(\text{py-pz})_3]^{2+}$ Complexes

compound	$\chi_m T_{300\text{K}}$
$[\text{Co}(\text{bpy})_3]^{2+}$	3.28
$[\text{Co}(\text{phen})_3]^{2+}$	3.23
$[\text{Co}(\text{bpy-pz})_2]^{2+}$	3.38
$[\text{Co}(\text{py-pz})_3]^{2+}$	3.16

HS octahedral Co(II) ions, as reflected by the $\chi_m T$ values at 300 K in the typical range of 2.8–3.4 $\text{cm}^3\cdot\text{K}\cdot\text{mol}^{-1}$, depending on the orbital contribution.⁸⁴ This HS configuration is further confirmed by the thermal variation of the product of the molar susceptibility times the temperature ($\chi_m T$) for $[\text{Co}(\text{bpy-pz})_2]^{2+}$ and $[\text{Co}(\text{py-pz})_3]^{2+}$. Both compounds show identical behaviors, with room-temperature $\chi_m T$ values of ca. 3.38 and 3.16 $\text{cm}^3\cdot\text{K}\cdot\text{mol}^{-1}$, respectively (Table 5). These values are higher than the spin-only one for an $S = 3/2$ spin ground state (1.875 $\text{cm}^3\cdot\text{K}\cdot\text{mol}^{-1}$) due to the orbital contribution of the ${}^4\text{T}_{1g}$ ground state of HS Co(II) ions. When the temperature is decreased the $\chi_m T$ product shows a continuous and smooth decrease, as a consequence of the first-order spin–orbit coupling arising from the ${}^4\text{T}_{1g}$ ground state.⁸⁴ This behavior suggests that both complexes are paramagnetic and present no interactions (see Figure 8a). Note that the slight differences in both plots can be attributed to the slightly different distortions of the octahedral geometry provided by the tris-bidentate and bis-tridentate coordination modes of the ligands in complexes

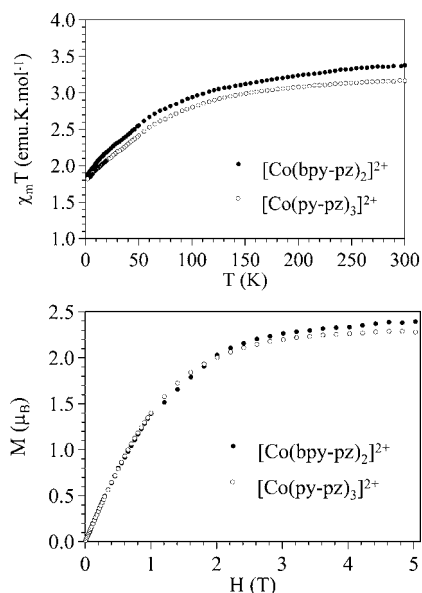


Figure 8. (a, top) Temperature dependence of the $\chi_m T$ product. (b, bottom) Isothermal magnetization at 2 K for the $[\text{Co}(\text{bpy-pz})_2]^{2+}$ and $[\text{Co}(\text{py-pz})_3]^{2+}$ complexes.

$[\text{Co}(\text{py-pz})_3]^{2+}$ and $[\text{Co}(\text{bpy-pz})_2]^{2+}$, respectively. The isothermal magnetization at 2 K for both compounds show also a very similar behavior and both samples reach a saturation value at high fields of ca. $2.3 \mu_B$ (Figure 8b). This value is below the expected one for a $S = 3/2$ spin ground state with $g = 2$ ($3 \mu_B$) and is attributed to the fact that at 2 K only the lowest Kramers doublet (arising from the splitting of the $^4T_{1g}$ term due to the first-order spin-orbit coupling) is populated and, therefore, the effective spin ground state is $1/2$. Assuming this $S = 1/2$ ground spin state the deduced effective g value is ca. 4.6 for both compounds, very close to those observed for other isolated HS Co(II) complexes.⁸⁴

As expected, the corresponding oxidation products of the four complexes in Table 5, i.e., complexes $[\text{Co}(\text{bpy})_3]^{3+}$, $[\text{Co}(\text{phen})_3]^{3+}$, $[\text{Co}(\text{py-pz})_3]^{3+}$, and $[\text{Co}(\text{bpy-pz})_2]^{3+}$, present LS Co(III) ions and are diamagnetic.

A survey of computational results are reported in Table 6, which show calculated oxidation potentials in good agreement with available experimental quantities. Interestingly, almost the same λ values (both LS and HS) are calculated for the tris-

bidentate $[\text{Co}(\text{R-bpy})_3]^{2+}$ and $[\text{Co}(\text{R-phen})_3]^{2+}$ complexes, in quantitative agreement with the average λ value reported in ref 34 obtained assuming a constant λ throughout the same series of cobalt complexes. In all these cases, essentially the same HS/LS energy splitting is calculated (recall the systematic error on this quantity) and the $^{LS}\lambda$ are much lower than the $^{HS}\lambda$, further corroborating the LS regeneration pathway. What is probably more surprising to observe in the calculated quantities is the almost total independence of the HS/LS splitting on the ligand donor strength, which is however capable of shifting the oxidation potential by more than 0.5 eV. Sizable variations in the HS/LS splitting are, on the other hand, observed when varying the ligand coordination from tris-bidentate to bis-tridentate. The $[\text{Co}(\text{bpy-pz})_2]^{2+}$ complex shows a HS/LS splitting comparable to that of the $[\text{Co}(\text{R-bpy})_3]^{2+}$ and $[\text{Co}(\text{R-phen})_3]^{2+}$ series, in agreement with the present magnetic susceptibility data, while the $[\text{Co}(\text{tpy})_2]^{2+}$ complex shows a LS ground state (see Table 6), consistent with previous magnetic data for this compound.^{41,42} A slight reduction (increase) of the $^{LS}\lambda$ ($^{HS}\lambda$) values is also calculated for $[\text{Co}(\text{bpy-pz})_2]^{2+}$ and for the $[\text{Co}(\text{tpy})_2]^{2+}$ complexes compared to the $[\text{Co}(\text{R-bpy})_3]^{2+}$ and $[\text{Co}(\text{R-phen})_3]^{2+}$ series.

Because the $[\text{Co}(\text{tpy})_2]^{2+/3+}$ complex shows the lower λ and a favored LS state, we speculate that this complex would give a faster regeneration of the oxidized dye compared to cobalt tris-bipyridyl and tris-phenanthroline complexes of the same oxidation potentials, as previously found for the analogous reaction studied in solution,⁵⁷ with ligand substitution allowing for fine-tuning of the complex oxidation potential. We also notice that a faster oxidized dye regeneration was reported for $[\text{Co}(\text{bpy-pz})_2]^{2+}$ compared to $[\text{Co}(\text{NO}_2\text{-phen})_3]^{2+}$, which feature essentially the same oxidation potential.^{17,34} These data are consistent with the calculated HS/LS and $^{LS}\lambda$ values for the two complexes, although the different electrolyte composition used in refs 17 and 34 could also contribute to the different behavior. Notice, however, that a very recent paper by Kashif et al. pointed out that a smaller reorganization energy could also lead to more rapid recombination between TiO_2 -injected electrons and Co(III) ions in the electrolyte.⁸⁶

4. CONCLUSIONS

We have reported a combined experimental and computational investigation to understand the nature of the interactions between cobalt redox mediators and TiO_2 surfaces sensitized by ruthenium and organic dyes, and their impact on the

Table 6. Oxidation Potential (ΔE_{OX}) and Reorganization Energies (λ) for the Doublet (LS) and Quartet (HS) Spin States Calculated for the Series of Different Investigated Cobalt Complexes

compound	R	ΔE_{OX}		$\Delta E_{\text{HS/LS}}$	$^{LS}\lambda$	$^{HS}\lambda$
		theor	expt			
$[\text{Co}(\text{R-bpy})_3]^{2+/3+}$	CH ₃	4.87	4.87 ^a	-0.22	0.63	1.36
	C(CH ₃)	4.85	4.87 ^a	-0.21	0.64	1.39
	H	5.06	5.00 ^a	-0.21	0.62	1.34
	Cl	5.42	N/A	-0.25	0.63	1.35
$[\text{Co}(\text{R-phen})_3]^{2+/3+}$	H	5.15	5.06 ^a	-0.24	0.61	1.31
	Cl	5.32	5.16 ^a	-0.23	0.62	1.30
	NO ₂	5.48	5.29 ^a	-0.25	0.60	1.30
$[\text{Co}(\text{py-pz})_2]^{2+/3+}$	H	5.42	5.40 ^b	-0.22	0.68	1.46
$[\text{Co}(\text{bpy-pz})_2]^{2+/3+}$	H	5.31	5.30 ^c	-0.19	0.59	1.57
$[\text{Co}(\text{tpy})_2]^{2+/3+}$	H	4.86	4.93 ^d	+0.05	0.51	1.37

^aData from ref 34. ^bFrom ref 85. ^cFrom ref 27. ^dFrom ref 51.

corresponding dye-sensitized solar cells' performances. We initially focused our attention on a series of Ru(II) dyes (N719 and Z907), to understand the reasons underlying the dramatic loss of efficiency observed for the prototype N719 dye in conjunction with cobalt electrolytes and to analyze the electron-transfer mechanism characterizing the dye regeneration process. We then extended the same concepts to a series of tailored organic dyes, for which we achieved a high photovoltaic efficiency of 6.5% with a cobalt electrolyte. Finally, a series of different cobalt complexes was investigated to trace structure/property relations and to cast possible guidelines for the design of high-performance cobalt-based electrolytes.

Both N719- and Z907-based DSSCs showed an increased lifetime in iodine-based electrolyte compared to the cobalt-based redox shuttle. In particular, we found that the N719 dye shows the shortest (longest) electron lifetimes in cobalt (iodine)-based electrolyte. By contrast, the organic dyes D21L6 and D25L6, endowed with long alkoxy chains, showed no significant change in the electron lifetime regardless of employed electrolyte and delivered high photovoltaic efficiency of 6.5% with a cobalt redox shuttle, by virtue of the enhanced DSSCs' open-circuit voltage.

To gain insight into the interaction between the cobalt electrolyte and the dye-sensitized TiO₂ interface, we carried out *ab initio* MD simulations of N719@TiO₂ in the presence of the oxidized [Co(bpy)₃]³⁺ species. The overall picture extracted from our dynamics simulation underlines the formation of a complex between the cobalt electrolyte and the surface-adsorbed dye which brings the [Co(bpy)₃]³⁺ species into contact with the TiO₂ surface. The driving force of this association is clearly the electrostatic attraction between the positively charged [Co(bpy)₃]³⁺ and the negatively charged carboxylates of the TiO₂-adsorbed N719 system. From the dynamics simulation we extracted three representative N719/[Co(bpy)₃]³⁺ structures, which have been further optimized in solution. Our data underline the effective formation of a rather strong Ru(II)⋯Co(III) ion-pair between N719 and [Co(bpy)₃]³⁺, with high values of binding energies in acetonitrile solution in the range 0.46–0.71 eV. The interaction between N719 and Co(III) ions was confirmed by the synthesis of the corresponding salt, which was insoluble in the organic solvents used for the electrolytes, and by NMR experiments in solution, showing interionic interactions between N719 and [Co(bpy)₃]³⁺. By using the calculated binding energies, we estimate a prevalence of Ru(II)⋯Co(II) couples for Z907, while the Ru(II)⋯Co(III) ion-pair for N719 is 10 times more abundant. This translates into an associated high probability of intercepting TiO₂-injected electrons by the oxidized [Co(bpy)₃]³⁺ species, lying close to the N719-sensitized TiO₂ surface. Notably, for all the investigated (neutral) organic dyes, we calculate almost zero binding energies with [Co(bpy)₃]³⁺, in line with the high reported photovoltaic performances.

Having calculated the structures of the interacting complexes, we simulated the possible Co(II)–Ru(III) couples formed after injection of one electron from the dye excited state to TiO₂, considering the possible spin states which are accessible for each couple, depending on the ferro- or anti-ferromagnetic coupling between ^{2/4}Co(II) and ²Ru(III), and evaluated the kinetics of the dye regeneration process in the Marcus theory framework. We found substantially different reorganization energies associated with the HS and LS cases, with calculated

values in the range 1.36–1.45 and 0.61–0.72 eV, respectively. The calculated reorganization energies for the ion-pairs are similar to those calculated for the doublet and quartet states of the isolated [Co(bpy)₃]²⁺ complex, with the isolated dyes all showing a ~0.1–0.2 eV reorganization energy for both organic and metallorganic systems. Lower activation energies are associated with the LS regeneration pathway, by virtue of the lower reorganization energies, in line with previous solution spectroscopic measurements on Co(II)→Ru(III) electron transfer.⁵⁷ This also implies that the spin-crossover equilibrium between the ⁴Co(II) and the ²Co(II) species and the rate of HS-to-LS conversion might be crucial to ensure a high concentration of the reactive LS species. Most notably, our calculated reorganization energies for the LS pathways (0.6–0.7 eV) are in excellent agreement with the average reorganization energy (0.8 ± 0.1 eV) recently reported by Feldt et al. for a series of cobalt complexes,³⁴ lending support to the proposed regeneration pathway. Furthermore, our model predicts ~7 times faster regeneration kinetics for N719 compared to Z907, in agreement with the 5 times faster regeneration half-times measured for N719 with respect to Z907.

Finally, we systematically investigated a series of [Co(R-bpy)₃]^{2+/3+} and [Co(R-phen)₃]^{2+/3+} complexes, and [Co(py-pz)₂]^{2+/3+}, [Co(bpy-pz)₂]^{2+/3+}, and [Co(tpy)₂]^{2+/3+}, to gauge the impacts of ligand substitution and metal coordination (tris-bidentate vs bis-tridentate) on the HS/LS energy difference and reorganization energies. Our results show almost the same reorganization energies for the tris-bidentate [Co(R-bpy)₃]²⁺ and [Co(R-phen)₃]²⁺ complexes, in quantitative agreement with the average λ values reported in ref 34. Surprisingly, we found the calculated HS/LS splitting and reorganization energies to be almost insensitive to the ligand donor strength, which is, however, capable of shifting the oxidation potential by more than 0.5 eV. This result was confirmed by magnetic susceptibility measurements that clearly indicated a HS state for the Co(II) complexes [Co(bpy)₃]²⁺, [Co(phen)₃]²⁺, [Co(py-pz)₂]²⁺, and [Co(bpy-pz)₂]²⁺, and a LS state for the corresponding Co(III) complexes [Co(bpy)₃]³⁺, [Co(phen)₃]³⁺, [Co(py-pz)₃]³⁺, and [Co(bpy-pz)₂]³⁺. Sizable variations in the HS/LS splitting are, on the other hand, observed when varying the ligand coordination from tris-bidentate to bis-tridentate, with a slight reduction of the reorganization energies calculated for the [Co(bpy-pz)₂]²⁺ and [Co(tpy)₂]²⁺ complexes, the latter showing a LS ground state. [Co(tpy)₂]^{2+/3+} being the complex showing the lower λ and a LS ground state, we speculate a faster regeneration of the oxidized dye compared to those with cobalt tris-bipyridyl and tris-phenanthroline complexes of same oxidation potential, with ligand substitution allowing for fine-tuning of the complex's oxidation potential.

■ ASSOCIATED CONTENT

📄 Supporting Information

Molecular orbitals, dye reorganization energies, optimized geometries, and NMR spectra. This material is available free of charge via the Internet at <http://pubs.acs.org>.

■ AUTHOR INFORMATION

Corresponding Author

filippo@thch.unipg.it

Notes

The authors declare no competing financial interest.

ACKNOWLEDGMENTS

We thank FP7-ENERGY-2010 Project ESCORT (contract no. 261023) for financial support of this work. E.M. and F.D.A. thank Fondazione Istituto Italiano di Tecnologia, Platform Computation, Project SEED 2009 "HELYOS" for a grant. C.J.G.G. thanks CTQ2011-26507 and Prometeo 2009/095 projects. C.Z. thanks the Ministero dell'Istruzione, dell'Università e della Ricerca (PRIN 2009 -LR88XR).

REFERENCES

- (1) (a) O'Regan, B.; Grätzel, M. *Nature* **1991**, *353*, 737–740. (b) Hagfeldt, A.; Boschloo, G.; Sun, L.; Kloo, L.; Pettersson, H. *Chem. Rev.* **2010**, *110*, 6595–6663. (c) Grätzel, M. *Acc. Chem. Res.* **2009**, *42*, 1788–1798. (d) Grätzel, M. *Nature* **2001**, *414*, 338–344.
- (2) Murakoshi, K.; Kano, G.; Wada, Y.; Yanagida, S.; Miyazaki, H.; Matsumoto, M.; Murasawa, S. *J. Electron. Chem.* **1995**, *396*, 27–34.
- (3) Bach, U.; Lupo, D.; Comte, P.; Moser, J. E.; Weissortel, F.; Salbeck, J.; Spreitzer, H.; Grätzel, M. *Nature* **1998**, *395*, 583–585.
- (4) Hagfeldt, A.; Didriksson, B.; Palmquist, T.; Lindström, H.; Södergren, S.; Rensmo, H.; Lindquist, S. *Sol. Energy Mater. Sol. Cells* **1994**, *31*, 481–488.
- (5) Boschloo, G.; Lindström, J.; Magnusson, E.; Holmberg, A.; Hagfeldt, A. *J. Photochem. Photobiol. A* **2002**, *148*, 11–15.
- (6) Nazeeruddin, M.; Kay, A.; Rodicio, I.; Humphry-Baker, R.; Müller, E.; Liska, P.; Vlachopoulos, N.; Grätzel, M. *J. Am. Chem. Soc.* **1993**, *115*, 6382–6390.
- (7) Nazeeruddin, M.; Pechy, P.; Renouard, T.; Zakeeruddin, S.; Humphry-Baker, R.; Comte, P.; Liska, P.; Cevey, L.; Costa, E.; Shklover, V.; Spiccia, L.; Deacon, G. B.; Bignozzi, C. A.; Grätzel, M. *J. Am. Chem. Soc.* **2001**, *123*, 1613–1624.
- (8) Nazeeruddin, M.; De Angelis, F.; Fantacci, S.; Selloni, A.; Viscardi, G.; Liska, P.; Ito, S.; Takeru, B.; Grätzel, M. *J. Am. Chem. Soc.* **2005**, *127*, 16835–16847.
- (9) Fukui, A.; Ryoichi, K.; Yamanaka, R.; Islam, A.; Han, L. *Sol. Energy Mater. Sol. Cells* **2006**, *90*, 649–658.
- (10) Lee, K. M.; Suryanarayanan, V.; Ho, K. C. *J. Power Sources* **2009**, *188*, 635–641.
- (11) Liyuan, H.; Ashraful, I.; Han, C.; Chandrasekharan, M.; Barredden, C.; Shufang, Z.; Xudong, Y.; Masatoshi, Y. *Energy Environ. Sci.* **2012**, *5*, 6057–6060.
- (12) Zeng, W.; Cao, Y.; Bai, Y.; Wang, Y.; Shi, Y.; Zhang, M.; Wang, F.; Pan, C.; Wang, P. *Chem. Mater.* **2010**, *22*, 1915–1925.
- (13) Rowley, J. G.; Farnum, B. H.; Ardo, S.; Meyer, G. J. *J. Phys. Chem. Lett.* **2010**, *1*, 3132–3140.
- (14) Boschloo, G.; Hagfeldt, A. *Acc. Chem. Res.* **2009**, *42*, 1819–1826.
- (15) O'Regan, B. C.; Walley, K.; Juozapavicius, M.; Anderson, A.; Matar, F.; Ghaddar, T.; Zakeeruddin, S. M.; Klein, C.; Durrant, J. R. *J. Am. Chem. Soc.* **2009**, *131*, 3541–3548.
- (16) Matar, F.; Ghaddar, T. H.; Walley, K.; DosSantos, T.; Durrant, J. R.; O'Regan, B. *J. Mater. Chem.* **2008**, *18*, 4246–4253.
- (17) Wang, M. K.; Chamberland, N.; Breaux, L.; Moser, J. E.; Humphry-Baker, R.; Marsan, B.; Zakeeruddin, S. M.; Grätzel, M. *Nat. Chem.* **2010**, *2*, 385–389.
- (18) Tian, H. N.; Jiang, X. A.; Yu, Z.; Kloo, L.; Hagfeldt, A.; Sun, L. *C. Angew. Chem., Int. Ed.* **2010**, *49*, 7328–7331.
- (19) Li, D. M.; Li, H.; Luo, Y. H.; Li, K. X.; Meng, Q. B.; Armand, M.; Chen, L. Q. *Adv. Funct. Mater.* **2010**, *20*, 3358–3365.
- (20) Liu, Y. R.; Jennings, J. R.; Parameswaran, M.; Wang, Q. *Energy Environ. Sci.* **2011**, *4*, 564–571.
- (21) Daeneke, T.; Kwon, T.-H.; Holmes, A. B.; Duffy, N. W.; Bach, U.; Spiccia, L. *Nat. Chem.* **2011**, *3*, 211–215.
- (22) Li, T. C.; Spokoyny, A. M.; She, C. X.; Farha, O. K.; Mirkin, C. A.; Marks, T. J.; Hupp, J. T. *J. Am. Chem. Soc.* **2010**, *132*, 4580–4582.
- (23) Sapp, S. A.; Elliott, C. M.; Contado, C.; Caramori, S.; Bignozzi, C. A. *J. Am. Chem. Soc.* **2002**, *124*, 11215–11222.
- (24) Nusbaumer, H.; Zakeeruddin, S. M.; Moser, J. E.; Grätzel, M. *Chem. Eur. J.* **2003**, *9*, 3756–3763.
- (25) Feldt, S. M.; Gibson, E. A.; Gabrielsson, E.; Sun, L.; Boschloo, G.; Hagfeldt, A. *J. Am. Chem. Soc.* **2010**, *132*, 16714–16724.
- (26) Cameron, P. J.; Peter, L. M.; Zakeeruddin, S. M.; Grätzel, M. *Coord. Chem. Rev.* **2004**, *248*, 1447–1453.
- (27) Yum, J.-H.; Baranoff, E.; Kessler, F.; Moehl, T.; Ahmad, S.; Bessho, T.; Marchioro, A.; Ghadiri, E.; Moser, J.-E.; Yi, C.; Nazeeruddin, M. D. K.; Grätzel, M. *Nat. Commun.* **2012**, *3*, 631.
- (28) Yella, A.; Lee, H.-W.; Tsao, H. N.; Yi, C.; Chandiran, A. K.; Nazeeruddin, M. D. K.; Diau, E. W.-G.; Yeh, C.-Y.; Zakeeruddin, S. M.; Grätzel, M. *Science* **2011**, *334*, 629–634.
- (29) Liu, Y.; Jennings, J. R.; Huang, Y.; Wang, Q.; Zakeeruddin, S. M.; Grätzel, M. *J. Phys. Chem. C* **2011**, *115*, 18847–18855.
- (30) Nusbaumer, H.; Moser, J. E.; Zakeeruddin, S. M.; Nazeeruddin, M. D. K.; Grätzel, M. *J. Phys. Chem. B* **2001**, *105*, 10461–10464.
- (31) Nelson, J. J.; Amick, T. J.; Elliott, C. M. *J. Phys. Chem. C* **2008**, *112*, 18255–18263.
- (32) Tsao, H. N.; Yi, C.; Moehl, T.; Yum, J.-H.; Zakeeruddin, S. M.; Nazeeruddin, M. D. K.; Grätzel, M. *ChemSusChem* **2011**, *4*, 591–594.
- (33) Ondersma, J. W.; Hamann, T. W. *J. Phys. Chem. C* **2010**, *114*, 638–645.
- (34) Feldt, S. M.; Wang, G.; Boschloo, G.; Hagfeldt, A. *J. Phys. Chem. C* **2011**, *115*, 21500–21507.
- (35) Gibson, E. A.; Smeigh, A. L.; Le Pleux, L.; Hammarström, L.; Odobel, F.; Boschloo, G.; Hagfeldt, A. *J. Phys. Chem. C* **2011**, *115*, 9772–9779.
- (36) DeVries, M. J.; Pellin, M. J.; Hupp, J. T. *Langmuir* **2010**, *26*, 9082–9087.
- (37) Nazeeruddin, M. D. K.; De Angelis, F.; Fantacci, S.; Selloni, A.; Viscardi, G.; Liska, P.; Ito, S.; Takeru, B.; Grätzel, M. *J. Am. Chem. Soc.* **2005**, *127*, 16835–16847.
- (38) Buscaino, R.; Baiocchi, C.; Barolo, C.; Medana, C.; Grätzel, M.; Nazeeruddin, M. K.; Viscardi, G. *Inorg. Chim. Acta* **2008**, *361*, 798–805.
- (39) Nazeeruddin, M. K.; Amirnasr, M.; Comte, P.; Mackay, J. R.; McQuillan, A. J.; Houriet, R.; Grätzel, M. *Langmuir* **2000**, *16*, 8525–8528.
- (40) De Angelis, F.; Fantacci, S.; Selloni, A. *Nanotechnology* **2008**, *19*, 424002.
- (41) (a) Krivokapic, I.; Zerara, M.; Dakua, M. L.; Vargas, A.; Enachescu, C.; Ambrusc, C.; Tregenna-Piggott, P.; Amstutz, N.; Krausz, E.; Hauser, A. *Coord. Chem. Rev.* **2007**, *251*, 364–378. (b) Goodwin, H. A. *Top. Curr. Chem.* **2004**, *243*, 23–47.
- (42) Vargas, A.; Zerara, M.; Krausz, E.; Hauser, A.; Daku, L. M. L. *J. Chem. Theory Comput.* **2006**, *2*, 1342–1359.
- (43) Newton, M. D. *Coord. Chem. Rev.* **2003**, *238*, 167–185.
- (44) Marcus, R. A. *J. Chem. Phys.* **1956**, *24*, 966–978.
- (45) Newton, M. D.; Sutin, N. *Annu. Rev. Phys. Chem.* **1984**, *35*, 437–480.
- (46) Buhks, E.; Bixon, M.; Jortner, J.; Navon, G. *Inorg. Chem.* **1979**, *18*, 2014–2018.
- (47) Larsson, S.; Ståhl, K.; Zerner, M. C. *Inorg. Chem.* **1986**, *25*, 3033–3037.
- (48) Newton, M. D. *J. Phys. Chem.* **1986**, *90*, 3734–3739.
- (49) Newton, M. D. *J. Phys. Chem.* **1991**, *95*, 30–38.
- (50) Torieda, H.; Yoshimura, A.; Nozaki, K.; Sakai, S.; Ohno, T. *J. Phys. Chem. A* **2002**, *106*, 11034–11044.
- (51) Torieda, H.; Nozaki, K.; Yoshimura, A.; Ohno, T. *J. Phys. Chem. A* **2004**, *108*, 4819–4829.
- (52) Nozaki, K.; Yoshimura, A.; Ohno, T. *Proc. Indian Acad. Sci. (Chem. Sci.)* **1993**, *105*, 495–503.
- (53) Song, X.; Lei, Y.; Wallendal, S. V.; Perkovic, M. W.; Jackman, D. C.; Endicott, J. F.; Rillema, D. P. *J. Phys. Chem.* **1993**, *97*, 3225–3236.
- (54) Creutz, C. J. *J. Phys. Chem. B* **2007**, *111*, 6713–6717.
- (55) Isied, S. S.; Vassilian, A.; Wishart, J. F.; Creutz, C.; Schwarz, H. A.; Sutin, N. *J. Am. Chem. Soc.* **1988**, *110*, 635–637.
- (56) Endicott, J. F.; Song, X.; Watzky, M. A.; Buranda, T. J. *Photochem. Photobiol. A: Chem.* **1994**, *82*, 181–190.
- (57) Yoshimura, A.; Uddin, M. J.; Amasaki, N.; Ohno, T. *J. Phys. Chem. A* **2001**, *105*, 10846–10853.

- (58) Perdew, J.; Burke, K.; Ernzerhof, M. *Phys. Rev. Lett.* **1996**, *77*, 3865–3868.
- (59) QUANTUM-ESPRESSO: Giannozzi, P.; Baroni, S.; Bonini, N.; Calandra, M.; Car, R.; Cavazzoni, C.; Ceresoli, D.; Chiarotti, G. L.; Cococcioni, M.; Dabo, I.; Dal Corso, A.; de Gironcoli, S.; Fabris, S.; Fratesi, G.; Gebauer, R.; Gerstmann, U.; Gougoussis, C.; Kokalj, A.; Lazzeri, M.; Martin-Samos, L.; Marzari, N.; Mauri, F.; Mazzarello, R.; Paolini, S.; Pasquarello, A.; Paulatto, L.; Sbraccia, C.; Scandolo, S.; Sclauzero, G.; Seitsonen, A. P.; Smogunov, A.; Umari, P.; Wentzcovitch, R. M. *J. Phys.: Condens. Matter* **2009**, *21*, 395502.
- (60) Martsinovich, N.; Jones, D. R.; Troisi, A. *J. Phys. Chem. C* **2010**, *114*, 22659–22670.
- (61) Frisch, M. J.; Trucks, G. W.; Schlegel, H. B.; Scuseria, G. E.; Robb, M. A.; Cheeseman, J. R.; Scalmani, G.; Barone, V.; Mennucci, B.; Petersson, G. A.; Nakatsuji, H.; Caricato, M.; Li, X.; Hratchian, H. P.; Izmaylov, A. F.; Bloino, J.; Zheng, G.; Sonnenberg, J. L.; Hada, M.; Ehara, M.; Toyota, K.; Fukuda, R.; Hasegawa, J.; Ishida, M.; Nakajima, T.; Honda, Y.; Kitao, O.; Nakai, H.; Vreven, T.; Montgomery, J. A., Jr.; Peralta, J. E.; Ogliaro, F.; Bearpark, M.; Heyd, J. J.; Brothers, E.; Kudin, K. N.; Staroverov, V. N.; Kobayashi, R.; Normand, J.; Raghavachari, K.; Rendell, A.; Burant, J. C.; Iyengar, S. S.; Tomasi, J.; Cossi, M.; Rega, N.; Millam, J. M.; Klene, M.; Knox, J. E.; Cross, J. B.; Bakken, V.; Adamo, C.; Jaramillo, J.; Gomperts, R.; Stratmann, R. E.; Yazyev, O.; Austin, A. J.; Cammi, R.; Pomelli, C.; Ochterski, J. W.; Martin, R. L.; Morokuma, K.; Zakrzewski, V. G.; Voth, G. A.; Salvador, P.; Dannenberg, J. J.; Dapprich, S.; Daniels, A. D.; Farkas, Ö.; Foresman, J. B.; Ortiz, J. V.; Cioslowski, J.; Fox, D. J. *Gaussian 09*, Revision A.1; Gaussian, Inc.: Wallingford, CT, 2009.
- (62) Becke, A. D. *J. Chem. Phys.* **1993**, *98*, 5648–5652.
- (63) (a) Cossi, M.; Barone, V. *J. Chem. Phys.* **2001**, *115*, 4708–4717. (b) Cossi, M.; Rega, N.; Scalmani, G.; Barone, V. *J. Comput. Chem.* **2003**, *24*, 669–681.
- (64) (a) McLean, A. D.; Chandler, G. S. *J. Chem. Phys.* **1980**, *72*, 5639–5648. (b) Raghavachari, K.; Binkley, J. S.; Seeger, R.; Pople, J. A. *J. Chem. Phys.* **1980**, *72*, 650–654.
- (65) (a) Dunning, T. H. Jr.; Hay, P. J. In *Modern Theoretical Chemistry*; Schaefer, H. F., III, Ed.; Plenum: New York, 1976; Vol. 3, pp 1–28. (b) Hay, P. J.; Wadt, W. R. *J. Chem. Phys.* **1985**, *82*, 270–283. (c) Wadt, W. R.; Hay, P. J. *J. Chem. Phys.* **1985**, *82*, 284–298. (d) Hay, P. J.; Wadt, W. R. *J. Chem. Phys.* **1985**, *82*, 299–311.
- (66) Reiher, O.; Salomon, O.; Hess, B. A. *Theor. Chem. Acc.* **2001**, *107*, 48–55.
- (67) Fantacci, S.; De Angelis, F. *Coord. Chem. Rev.* **2011**, *255*, 2704–2726.
- (68) Krist, K.; Gafney, H. D. *J. Phys. Chem.* **1982**, *86*, 951–958.
- (69) Nazeeruddin, Md. K.; Zakeeruddin, S. M.; Humphry-Baker, R.; Jirousek, M.; Liska, P.; Vlachopoulos, N.; Shklover, V.; Fischer, C.-H.; Grätzel, M. *Inorg. Chem.* **1999**, *38*, 6298–6305.
- (70) Wang, P.; Zakeeruddin, S. M.; Moser, J. E.; Nazeeruddin, Md. K.; Sekiguchi, T.; Grätzel, M. *Nat. Mater.* **2003**, *2*, 402–407.
- (71) Hagberg, D. Doctoral Thesis, KTH, 2009.
- (72) Yum, J.-H.; Hagberg, D. P.; Moon, S.-J.; Karlsson, K. M.; Marinado, T.; Sun, L.; Hagfeldt, A.; Nazeeruddin, Md. K.; Grätzel, M. *Angew. Chem., Int. Ed.* **2009**, *48*, 1576–1580.
- (73) Moon, S.-J.; Yum, J.-H.; Humphry-Baker, R.; Karlsson, K. M.; Hagberg, D. P.; Marinado, T.; Hagfeldt, A.; Sun, L.; Grätzel, M.; Nazeeruddin, Md. K. *J. Phys. Chem. C* **2009**, *113*, 16816–16820.
- (74) Ito, S.; Murakami, T. N.; Comte, P.; Liska, P.; Grätzel, M.; Nazeeruddin, M. K.; Grätzel, M. *Thin Solid Films* **2008**, *516*, 4613–4619.
- (75) O'Regan, B. C.; Lenzmann, F. *J. Phys. Chem. B* **2004**, *108*, 4342–4350.
- (76) Marcus, Y.; Hefter, G. *Chem. Rev.* **2006**, *106*, 4585–4621.
- (77) Bottomley, G. A.; Glossop, L. G. *J. Electroanal. Chem.* **1981**, *118*, 433.
- (78) Duffy, N. W.; Peter, L. M.; Rajapakse, R. M. G.; Wijayantha, K. G. U. *J. Phys. Chem. B* **2000**, *104*, 8916–8919.
- (79) (a) De Angelis, F.; Fantacci, S.; Selloni, A.; Nazeeruddin, Md. K.; Grätzel, M. *J. Phys. Chem. C* **2010**, *114*, 6054–6061. (b) De Angelis, F.; Fantacci, S.; Selloni, A.; Nazeeruddin, Md. K.; Grätzel, M. *J. Am. Chem. Soc.* **2007**, *129*, 14156–14157.
- (80) Griffith, M. J.; James, M.; Triani, G.; Wagner, P.; Wallace, G. G.; Officer, D. L. *Langmuir* **2011**, *27*, 12944–12950.
- (81) (a) Tribollet, R.; Malini-Balakrishnan, R.; Sigel, H. *J. Chem. Soc., Dalton Trans.* **1985**, 2291–2303. (b) Newcomb, L. F.; Gellman, S. H. *J. Am. Chem. Soc.* **1994**, *116*, 4993–4994. (c) McGaughey, G. B.; Gagné, M.; Rappé, A. K. *J. Biol. Chem.* **1998**, *273*, 15458–15463.
- (82) Clifford, J. N.; Palomares, E.; Nazeeruddin, Md. K.; Grätzel, M.; Durrant, J. R. *J. Phys. Chem. C* **2007**, *111*, 6561–6567.
- (83) Lobello, M. G.; Fantacci, S.; De Angelis, F. *J. Phys. Chem. C* **2011**, *115*, 18863–18872.
- (84) (a) Shi, Z.; Peng, J.; Gómez-García, C. J.; Benmansour, S.; Gu, X. *J. Solid State Chem.* **2006**, *179*, 253–265. (b) Humphrey, S. M.; Alberola, A.; Gómez-García, C. J.; Wood, P. T. *Chem. Commun.* **2006**, 1607–1609. (c) Gómez-García, C. J.; Coronado, E.; Borrás-Almenar, J. J. *Inorg. Chem.* **1992**, *31*, 1667–1673. (d) Benmansour, S.; Setifi, F.; Gómez-García, C. J.; Triki, S.; Coronado, E.; Salaün, J. Y. *J. Mol. Struct.* **2008**, *890*, 255–262. (e) Liu, H.; Gómez-García, C. J.; Peng, J.; Sha, J.; Wanga, L.; Yan, Y. *Inorg. Chim. Acta* **2009**, *362*, 1957–1962. (f) Lloret, F.; Julve, M.; Cano, J.; Ruiz-García, R.; Pardo, E. *Inorg. Chim. Acta* **2008**, *361*, 3432–3445.
- (85) Ahmad, S.; Bessho, T.; Kessler, F.; Baranoff, E.; Frey, J.; Chenyi, Yi, C.; Grätzel, M.; Nazeeruddin, M. K. *Phys. Chem. Chem. Phys.* **2012**, *14*, 10631–10639.
- (86) Kashif, M. K.; Axelson, J. C.; Duffy, N. W.; Forsyth, C. M.; Chang, C. J.; Long, J. R.; Spiccia, L.; Bach, U. *J. Am. Chem. Soc.* **2012**, *134*, 16646–16653.